Construction and Building Materials 264 (2020) 120158

Contents lists available at ScienceDirect

Construction and Building Materials

journal homepage: www.elsevier.com/locate/conbuildmat

Optimization and mechanical-physical characterization of geopolymers with Construction and Demolition Waste (CDW) aggregates for construction products

Matteo Panizza [a,*], Marco Natali [a], Enrico Garbin [b], Vilma Ducman [c], Sergio Tamburini [a]

[a] National Research Council of Italy (CNR), Institute of Condensed Matter Chemistry and Technologies for Energy (ICMATE), Corso Stati Uniti 4, 35127 Padova, Italy
[b] University of Padova, Inter-Departmental Research Centre for the Study of Cement Materials and Hydraulic Binders (CIRCe), Via G. Gradenigo 6, 35131 Padova, Italy
[c] Slovenian National Building and Civil Engineering Institute (ZAG), Dimičeva ulica 12, 1000 Ljubljana, Slovenia

HIGHLIGHTS

- Geopolymers with CDW aggregates were optimized for producing architectural panels.
- Final materials were characterized from a mechanical and physical standpoint.
- Aspect ratio and size of specimens were compared to concrete/mortar provisions.
- Splitting was correlated to compressive strength through numerous tested geopolymers.
- Recyclability of geopolymers as waste aggregates was preliminarily assessed.

GRAPHICAL ABSTRACT

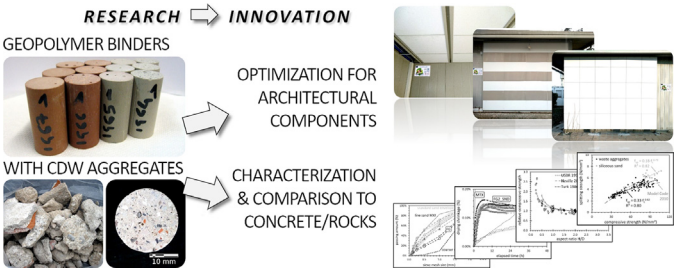

ARTICLE INFO

Article history:
Received 25 September 2019
Received in revised form 4 July 2020
Accepted 6 July 2020
Available online 28 July 2020

Keywords:
Geopolymers
Alkali-Activated Materials (AAM)
Construction and Demolition Waste (CDW)
Building Materials
Recycled Aggregates
Mortar
Concrete
Compressive strength
Tensile strength
Shrinkage

ABSTRACT

The paper presents the mechanical and physical characterization of a metakaolin-slag-fly ash-potassium silicate geopolymer mortar embedding inorganic recycled aggregates from Construction and Demolition Waste (CDW). The binder was holistically optimized to comply with the pilot plant requirements for producing architectural panels of satisfactory quality, among them: reduced viscosity, minimum open time of 1 h, use of commercial reagents, sufficient strength and limited shrinkage. Size and aspect ratio of small scale cylindrical specimens were investigated in compression, comparing the performance of tested geopolymers to available provisions for natural rocks, cement concrete and mortars. Empirical correlations between compressive and splitting tensile strength were calibrated through the results of about 130 geopolymer mixtures produced in former and current activities. Lastly, the suitability of reusing geopolymers at their end-of-life as recycled aggregates in a new geopolymer production was preliminarily assessed to explore the feasibility of a closed-loop process.

* Corresponding author.
E-mail addresses: matteo.panizza@icmate.cnr.it (M. Panizza), marcostefano.natali@cnr.it (M. Natali), enrico.garbin@unipd.it (E. Garbin), vilma.ducman@zag.si (V. Ducman), sergio.tamburini@cnr.it (S. Tamburini).

https://doi.org/10.1016/j.conbuildmat.2020.120158
0950-0618/

1. Introduction

The Construction sector generates approximately one third of the total waste produced yearly in the European Union (EU-28), and non-hazardous waste from construction and demolition represents more than 10% (about 335 million tonnes in 2016) of the overall European waste stream [1]. Construction and Demolition Waste (CDW) typically includes large quantities of inorganic materials like concrete, bricks, tiles and ceramics, with smaller amounts of other components [2,3]. Although the minimum target of preparation for reuse, recycling and other material recovery of CDW, set by the Waste Framework Directive [4] at 70% by weight within 2020, has already been or is going to be accomplished in most EU-28 Countries [1], it is worth highlighting that it includes backfilling operations. CDW is potentially relevant for recovery and reuse, and its recycling is environmentally significant since it would reduce CO_2 emissions, consumption of energy and natural resources, and would preserve valuable space in landfills as well [3,5]. Typically, the main destinations of recycled CDWs are unbound aggregates for road sub-bases [6], and bound aggregates for concrete mixes [7–9], the latter being a higher added value recycling pathway.

The manufacturing of structural Recycled Aggregates Concrete (RAC) comparable to standard concrete is not unfeasible, but it requires a careful optimization of CDW typologies [10,11], grading [12] and concrete mix design [13], thanks to an improved refinement of the Interfacial Transition Zone (ITZ) between old aggregates and the new cementitious matrix [14,15]. Nevertheless, the use of RAC is restrained by several drawbacks, such as a larger water absorption of recycled aggregates that affects mix design and preparation, inferior mechanical properties and greater drying shrinkage generally exhibited by RACs in comparison to concrete made with natural aggregates, an often lower resistance to carbonation and chloride penetration, and the still low cost of natural aggregates [7–10]. In addition, most researches and applications involved the use of concrete waste aggregates, whereas brick and masonry rubble has been less investigated, mostly in the '40s and '50s as a consequence of the abundant debris left by World War II [16], owing to their features in terms of apparent density, porosity and water absorption that bring additional issues [17,18].

The use of CDW in Alkali Activated Materials (AAM) and geopolymer binders, as either inert aggregates or partially reactive materials, has been investigated in the last years with encouraging results [19,20]. AAM/geopolymers showed a remarkable flexibility in using numerous types of different industrial wastes and by-products [21,22], and seem to offer a promising alternative recycling option for CDW as well. Concrete and/or fired clay waste aggregates were studied in several researches [23–27]. Concrete, brick, glass and ceramic tile waste in geopolymer binders were investigated as well [28–30], whereas brick waste aggregates alone were studied by Robayo-Salazar et al. [31] and Reig et al. [32], and ceramic waste aggregates were tested by Puertas et al. [33] and Sun et al. [34]. These studies testify both the interest and the potential of AAM/geopolymer binders in the recycling of CDW. Nonetheless, in most cases the published researches do not tackle, concurrently and comprehensively, aspects related to technological features of the fresh paste, to physical properties and mechanical performance of the hardened material, and to recycling potential.

Within this context, the Horizon 2020 European RIA project InnoWEE – "Innovative pre-fabricated components including different waste construction materials reducing building energy and minimising environmental impacts" – started in 2016 – developed architectural panels for external insulation, for ventilated façades and for interior radiant hydronic heating/cooling, made with geopolymer mixtures embedding up to 50% of inorganic CDW aggregates. These prefabricated components aim at improving the energy performance of buildings, which account for about 40% of the total energy consumption in the European Union [35] and are deemed strategic in the frame of EU policies towards the improvement of Europe's energy security, competitiveness and sustainability.

The preliminary assessment of InnoWEE mixtures was presented in Panizza et al. [36], where their suitability for industrial production was tested by exploring various parameters assumed to affect the subsequent scaled-up process (e.g. nature, amount and particle size distribution of waste aggregates, metakaolin:slag ratio, curing temperature, etc.). This paper reports the follow-up research carried out to optimize the formulation for a pourable mortar suitable for the pilot production of InnoWEE panels, conceived and carried out by a partner of the InnoWEE consortium, which consisted of about 400 items for installation in four demo buildings. As an example, a description of prototyping, production and testing of external insulation panels is given in Frankovič et al. [37]. More in detail, the requirements for the binder included a viscosity low enough to allow flowing by gravity, a minimum open time of 1 h at room temperatures lower than 23 °C, the use of readily available commercial reagents, and the achievement of adequate values of strength and drying shrinkage. The performance of the hardened mortar was deemed acceptable when it yielded panels with a satisfactory quality, in terms of limited defects (e.g. cracks and geometry distortions) and compliance to current regulations for non-structural components.

The innovative holistic approach involved not only physical and mechanical properties of the hardened material, but also technological properties of the fresh paste, controlling at the same time the thermal features needed to enable the production of radiant panels.

From a methodological point of view, the suitability of small-scale cylindrical specimens was extensively investigated in uniaxial compression with regard to diameter size and aspect ratio, with the aim of comparing results to the current knowledge of natural rocks and cement concrete/mortars, thus supporting the soundness of outcomes. Additionally, a database of about 130 geopolymer-based materials, tested in past and present activities, was gathered to establish empirical correlations between compressive and splitting tensile strength, which is relevant from a design standpoint. This systematic exploration of mechanical performance, aimed at providing valuable knowledge for desirable standardization purposes, is unprecedented with regard to geopolymer or AAM materials.

Lastly, the possible end-of-life reuse of geopolymer waste, as recycled aggregates in a new production of the same material, was preliminarily assessed from a mechanical standpoint in order to support a virtual feasibility of a closed-loop process, not yet taken into consideration in the field of geopolymers/AAM, and possibly neither in the case of ordinary concrete.

Through this paper, the term "geopolymer" was used instead of the more general "AAM", according to Provis et al. [38], thanks to the primary role of the aluminosilicate and highly coordinated binding phase.

2. Overview of the experiments

2.1. Materials

2.1.1. Precursors and activators

The geopolymer binder was prepared by mixing commercial metakaolin, either MK0 (median particle size D_{50} = 8.6 μm) or MK1 (D_{50} = 15.6 μm), commercial ground-granulated blast-

Table 1
Elemental analysis by oxides (% weight) of metakaolin (MK), furnace slag (SL) and class F fly ash (FA).

Material	Al_2O_3	CaO	Fe_2O_3	K_2O	Na_2O	MgO	SiO_2	SO_3	TiO_2	Others
MK0	39.08	–	1.78	0.94	–	–	56.16	–	2.04	–
MK1	41.47	–	1.97	1.18	–	0.15	53.26	–	1.95	–
SL	9.31	44.36	0.57	0.71	–	6.20	36.48	1.55	0.83	–
FA0	28.45	5.44	10.38	2.57	1.49	2.65	45.97	1.53	1.53	–
FA1	24.81	6.52	7.16	2.51	1.42	2.32	50.51	1.72	1.43	1.60

furnace slag (SL, with D_{50} = 9 μm), and class F fly ash, either FA0 coming from an Italian power plant in Brindisi and used in preliminary testing, or FA1 from Germany, the latter having D_{50} = 17.9 μm, as reported in their datasheet. MK0 and MK1 originate from the same raw materials through rotary kiln calcination, and basically differ in their milling phase, the former being finer than the latter. The quantitative chemical analysis of the precursors by Energy Dispersive X-ray Spectrometry (EDS) is reported in Table 1.

Potassium silicate activators with a molar modulus (MM) SiO_2/K_2O comprised between 1.4 and 2.4 were prepared in-house by mixing a 50%w colloidal silica dispersion and KOH pellets with distilled water at least 24 h prior to use. The dry matter concentration was either 42%, 45% or 50%. All the potassium silicate solutions were analysed according to an internal protocol, treating the solution with NaF and titrating the acid/base excess, together with EDS analysis to verify the presence of Na. Based on the chemical composition of the reagents (not taking into account waste aggregates), with reference to the mixtures herein presented in details, the generic Si/Al molar ratios of the activator and the solid precursors were comprised between 2.1 and 2.6, with K/Si comprised between 0.26 and 0.38 and K/Al between 0.55 and 0.88.

2.1.2. Waste aggregates

Waste aggregates were obtained from non-hazardous inorganic CDW coming from selective demolitions of ordinary buildings carried out by a partner of the InnoWEE consortium, operating in the field of recycled aggregates for road backfilling and responsible also for the processing of waste. Input CDW materials, classified either as 17.01.01 (concrete), 17.01.07 (mixtures of concrete, bricks, tiles and ceramics), or 17.09.04 (mixed construction and demolition wastes), according to the European List of Wastes [39], were ground to produce recycled sands with maximum size of 2 mm. Generally, the filler fraction below 63 μm, produced during milling, was not removed. In preliminary phases, scraps of concrete (EWC code 17.01.01 – concrete) and fired clay (EWC code 17.01.02 – bricks) were milled separately to obtain reference aggregates, i.e. CR1 and FC1 [36]. Subsequently, mixed rubble was ground together to produce a blend of waste aggregates with various sizes, namely a 0–2 mm sand (MX1), a fine sand 0–1 mm (MXf) and a coarser sand 1–2 mm (MXc). MXf and MXc were then combined in various proportions to obtain the input waste aggregates labelled as FG1/FG2. For collateral testing, two sets of residual cubic test specimens of ordinary Portland cement concrete with natural aggregates, one of them including steel mill slag sand (labelled CR2 and CR3, respectively), were milled, and size fractions were kept separated to be recombined prior to use with a Particle Size Distribution (PSD) matching that of either CR1 or FG2.

In addition, three batches of recycled geopolymer aggregates (RG) were obtained by crushing residual test specimens produced during previous and present activities, with most of the original materials that contained approximately 50% of either the former waste or natural sand aggregates. RG3 was obtained from test specimens of mixtures made with about 50%dw of concrete aggregates CR2 and CR3.

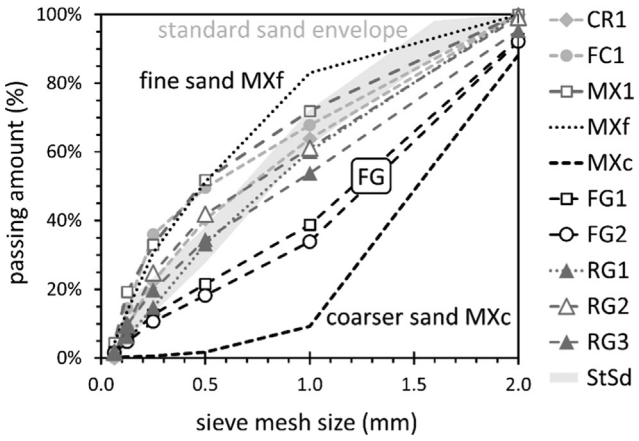

Fig. 1. Measured Particle Size Distributions (PSDs) of processed CDW.

Representative samples from processed CDW were screened with woven wire cloth sieves having a square mesh size complying with EN 933-2 [40] (apertures from 0.063 mm to 2 mm), in order to measure their PSD. Outcomes are shown in Fig. 1, which reports also the aggregate distributions used for the final formulations (FG).

2.1.3. Preparation of binders and specimens

Powder reagents (i.e. metakaolin, slag and fly ash) were stirred together with the alkali activator in an 8 l planetary mixer for about 5 min. Then, aggregates were added, together with possible extra water. Mixtures were stirred for further 3–5 min. Short fibres, if required, were dispersed into the paste 2 min before the end of the mixing. When ready, the geopolymer mixture was cast into plastic pipes with a nominal internal diameter of 22 mm. When required, small pneumatic ball vibrators were used to accelerate the spread of the paste and to promote the expulsion of possible air bubbles entrapped. Pipes were then sealed with masking tape and placed inside plastic bags, closed carefully to prevent a premature evaporation of water. Unless otherwise specified, specimens were cured for 12°h either in oven or in a conditioned room at 20 °C, assumed as ambient temperature curing. Cylinders were demoulded after one day, and placed until testing in a conditioned room at 20 °C inside their resealed plastic bags, which were opened after three days to allow cutting of specimens and to promote the evaporation of water.

2.1.4. Test summary and composition of geopolymer binders

The present investigation involved 37 mixtures tested in compression and splitting at least at 7 and 28 days of age, with 10 of them tested at 3 days and 21 up to 6 months (2 up to 1 year). Density, open porosity and water absorption were measured for all materials after at least 3–4 months of curing. Unless otherwise stated, 3 repetitions per test were carried out.

Mixtures can be grouped according to four main topics: (i) reference thixotropic materials, based on PSDcr-r and PSDfc-r studied in Panizza et al. [36]; (ii) mixtures for studying fluidity and open

Table 2
Composition of the tested binders, with corresponding labels. Water content and type of aggregates may vary. Molar ratios are reported for the elements, rounded to two significant figures.

K-silicate		Powder reagents (% dry weight)					Binder	
SiO_2/K_2O	Concentr.	Metakaolin		Slag	Fly Ash		Si/Al	K/Al
Reference thixotropic mixtures								
Labels: REF_wCR1; REF_wCR2; REF_wCR3; REF_wMX; REF_wFG								
1.8	45%	18.4%	(MK1)	18.4%	–		2.3	0.75
Study of fluidity and open time								
Labels: FL-A; FL-B; FL-C; FL-D								
2.3	42%	18.4%	(MK0)	18.4%	–		2.4	0.66
Label: FL-E								
2.3	42%	17.8%	(MK0)	17.8%	–		2.6	0.81
Label: FL-F								
1.4	45%	18.5%	(MK0)	18.5%	–		2.2	0.84
Labels: FLfa-A; FLfa-B								
2.3	42%	18.4%	(MK0)	9.2%	9.2%	(FL0)	2.1	0.55
Label: FLfa-C								
2.3	42%	17.8%	(MK0)	8.9%	8.9%	(FL0)	2.2	0.68
Label: FLfa-D								
2.3	42%	18.4%	(MK0)	13.8%	4.6%	(FL0)	2.2	0.60
Use of commercial reagents								
Label: FL-B2								
2.3	42%	18.4%	(MK1)	18.4%	–		2.2	0.63
Label: FLfa-B2								
2.3	42%	18.4%	(MK1)	9.2%	9.2%	(FL1)	2.1	0.55
Labels: Ksd-A; Ksd-B								
2.3	42%	16.6%	(MK1)	16.6%	–		2.2	0.63 (A) 0.69 (B)
Labels: Kwa-A; Kwa-B								
2.3	42%	18.3%	(MK1)	18.3%	–		2.2	0.63 (A) 0.69 (B)
Final materials								
Labels: FG1; FG1_NFB; FG2; FG2_CNT; FG2_30; FG2_20; FG2_NFA*; FG2_WT1/2; FG2_CR2/3; FG2_SND; RGA1/2/3								
1.9	45%	17.8%	(MK1)	11.9%	5.9%	(FL1)	2.2	0.80
Collateral testing (curing temperature). Label: IG1								
2.4	45%	18.4%	(MK0)	18.4%	–		2.4	0.63

* Fly ash replaced by slag – Si/Al ~ 2.3, K/Al ~ 0.88.

time; (iii) use of commercial reagents, with comparison of two types of metakaolin and K-silicate either in-house prepared or commercially available; (iv) optimized final recipe, with variations of parameters such as curing temperature, nature of aggregates, water content, etc.

The type of K-silicate and the proportions of reagents, used in the binder of mixtures mentioned in details in this paper, are reported in Table 2, together with the corresponding molar ratios of Si/Al and K/Al based on the chemical composition of alkali activator and powder reagents, not including waste or sand aggregates and not making assumptions on the actual reactivity of precursors. The amount of aggregates was about 50% of dry weight for all the materials. Water content and nature of aggregates are reported in the relevant sections.

2.2. Test methods

2.2.1. Compressive, splitting and bending strength

Uniaxial compression tests, splitting tests (also known as Brazilian tests) and 3-point bending tests were carried out, according to the main principles of standards EN 12390-3 [41], EN 12390-6 [42] and EN12390-5 [43], with a 50 kN universal electro-mechanic multipurpose frame equipped either with a 50 kN load cell (compression and splitting) or a 2.5 kN load cell (bending). Cylindrical specimens with a nominal diameter of 22 mm, and a nominal height of either 44 mm in compression or 22 mm in splitting, were used in compression and splitting tests. Plates 120 mm long, 22 mm wide and 15 mm thick were tested in 3-point bending with a span of 100 mm. The actual dimensions were measured with a resolution of 0.05 mm. The size was a trade-off between economy of mixtures and representativeness of results, consistently with the previous research reported in Panizza et al. [36]. Nonetheless, although the minimum size of compression specimens was more than 10 times the maximum aggregate size D_{max} (2 mm) and the aspect ratio of 2 should allow measuring the cylinder strength, as already discussed [36], a preliminary assessment in compression was carried out on larger samples with diameter 35 mm, and the height-to-diameter ratio was explored within the range 0.25–3 as well (Section 5).

The top and bottom surfaces of specimens to be tested in compression were ground to improve the contact with the steel plates of the machine. Due to the small size of specimens for splitting tests, packing strips were not used, but four layers of 80 g/m^2 paper were placed instead, to improve the contact. Soft putty for glass windows was used to keep samples in position after being centred between the plates, and it was removed during the test. The upper and lower faces of bending specimens were smoothed, in correspondence of the cylindrical supports, to prevent an uneven loading.

All tests were carried out in displacement control, with a rate of the movable transverse beam of either 0.5 mm/min (compression), 0.3 mm/min (splitting) or 0.1 mm/min (bending), in order to ensure a quasi-static application of the load and a reasonable duration of about 3–5 min for most tests. The maximum load was recorded for calculating compressive strength f_c (Eq. (1), were P_{max} is the failure load and A_c is the cross-sectional area of the specimen on which the compressive force acts), splitting strength f_{sp} (Eq. (2), where d and L are the average diameter and length in correspondence of the diametral plane under loading) and bending strength f_b (Eq. (3), where s is the span between supports, b and h are specimen width and thickness, respectively).

$$f_c = \frac{P_{max}}{A_c} \quad (1)$$

$$f_{sp} = \frac{2 \cdot P_{max}}{\pi \cdot L \cdot d} \quad (2)$$

$$f_b = \frac{3 \cdot P_{max} \cdot s}{2 \cdot b \cdot h^2} \quad (3)$$

2.2.2. Dry bulk density, material density, open porosity and water absorption

The measure of dry bulk density (ρ_b), material density (ρ_m), open porosity (OP) and water absorption (WA) was carried out, according to the main principles of ASTM C20-00 [44], on samples obtained by cutting disks about 8–12 mm thick from the cylinders with a nominal diameter of 22 mm used for compression and splitting tests. An analytical balance (accuracy class I, scale interval $2 \cdot 10^{-4}$ g), equipped with a set of tools for the determination of density through the buoyancy method, was used for weighing operations. Dry bulk density is herein defined as the ratio of dry weight and exterior volume (pores included), while material density is the ratio of dry weight and volume of impervious portions. The open porosity represents the amount of pores accessible by water, expressed as a percentage of the exterior volume, and the water absorption is the ratio between weight of water absorbed by the saturated specimen and weight of the dry specimen.

Specimens were immersed in demineralized water for 24 h and subsequently boiled for at least 2 h, in order to assure their complete saturation and to leach out possible soluble salts. Then, their saturated weight (W) and the weight while suspended in water (S) were recorded, taking care to keep them immersed during the operations. Finally, the dry weight (D) was obtained after drying in oven at 105–110 °C until constant weight. Properties were calculated as in Eqs. (4)–(7) [44]. In addition, the apparent density in environmental conditions (ρ_{ap}) was calculated as the ratio of mass and exterior volume measured on specimens for compression tests.

$$\rho_b = \frac{D}{W - S} \quad (4)$$

$$\rho = \frac{D}{D - S} \quad (5)$$

$$OP = \frac{W - D}{W - S} \quad (6)$$

$$WA = \frac{W - D}{D} \quad (7)$$

2.2.3. Measurement of drying shrinkage

The measurement of drying shrinkage was carried out on cylindrical specimens 160 mm long with diameter 22 mm, placed vertically inside frames specifically designed, supporting a digital dial gauge (resolution 1 μm and accuracy 3 μm) mounted in contact with the top end of the specimen. The bottom end was supported by a spherical restraint at the central axis of the cylinder. In order to prevent a premature onset of drying shrinkage, specimens were kept wrapped in wet paper and sealed inside plastic bags immediately after casting and during the 6-day curing phase after demoulding, as done for panel prototypes. Since transducers were not equipped with a data acquisition system, displacements were automatically recorded by means of a full-HD webcam programmed to take snapshots with variable frequency (every 15–60 min during the first 12–24 h of drying, every 2–4 h afterward). Due to the limited number of transducers and frames available (i.e. 5), one specimen per batch of mixture was monitored, in a continuous fashion for at least the first 2–7 days (or up to 4–6 weeks when possible), then removed and occasionally replaced for 1–2 days at least, ensuring that the position did not change thanks to a reference mark.

Although measurements were carried out in a conditioned environment set at 20 °C, room temperature and relative humidity could not be strictly controlled and daily fluctuations occurred, thus preventing the application of a standard. Nonetheless, a monitoring carried out over 60 days between February and April, with data logged every 15 min, delivered the following results (mean ± s.d.): temperature 20.7 ± 0.9 °C, with more than 90% of values falling in the range 19.0–22.0 °C; relative humidity 43.0 ± 8.8%, with more than 90% of values in the range 28.0–58.0%. A rigorous determination of dry shrinkage properties, however, was not a purpose of the investigation, since testing was aimed at highlighting differences among mixtures, and was supported by heuristic observations of real scale panel prototypes produced in parallel.

3. Tuning of properties for the pilot production

3.1. Curing temperature

In the previous research [36], focused on viscous thixotropic mixtures, curing temperatures in the range 20–60 °C were found to affect mostly the early-age strength gain (24 h–7 days), with a negligible difference in the long-term. For this reason, the curing was initially set at 30 °C, a temperature that can be easily controlled with a relatively low energy expenditure. It is to be noted that the drying shrinkage test setup was not available yet. As the prototyping phase began, drying shrinkage was disclosed as one of the main sources of defects. The effect of initial curing temperatures on shrinkage was therefore studied on two mixtures, REF_wCR1 (formerly labelled PSDcr-r [36]) with concrete waste aggregates and IG1 with a blend of concrete and fired clay aggregates in 1:1 proportion. Results, plotted in Fig. 2 and listed in Table 3, showed the effectiveness of higher curing temperatures in reducing the drying shrinkage, with a decrease from 20 to 60 °C of about 50% of the maximum value recorded in 2 days and in 5 weeks. On the other hand, there was little improvement between 50 and 60 °C, being the difference approximately 5–7%. Consequently, a 12-hour curing temperature of 50 °C combined with a 6-day humid curing phase at room temperature was selected as a suitable trade-off for prototypes and scaled-up production. Indeed, higher temperatures are known to foster the consolidation of the geopolymer network and its porosity, promoting a faster expulsion of water [45]. In addition, short plastic fibres 6 mm long (initially 1.2‰ of dry weight of polyacrylonitrile – PAN, subsequently 1.5‰ of dry weight of polypropylene – PP) were added to counteract possible shrinkage cracks.

3.2. Open time and fluidity

The open time, herein intended as the time spanning from beginning of reaction (i.e. from mixing alkali activator and powder reagents) and loss of pourability, was determined by qualitative observations, while viscosity was measured with a rotational viscometer (spindle n°5 at 1 rpm).

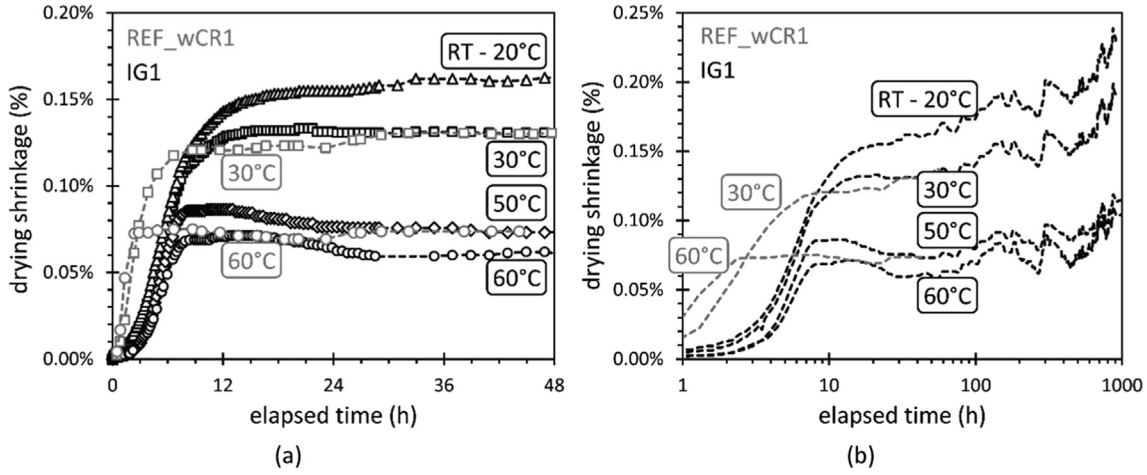

Fig. 2. Effect of initial curing temperature on drying shrinkage: (a) first 48 h and (b) up to 6 weeks.

Table 3
Maximum recorded values of shrinkage, rounded to 2 significant figures, related to curing temperatures for reference mixtures (*h* stands for hours and *w* for weeks).

Mixture	Curing temp. °C	48 h max shrinkage	Δ	5 w max shrinkage	Δ
REF_wCR1	20	0.14%		–	
	60	0.08%	−45%	–	
IG1	20	0.16%		0.24%	
	30	0.13%	−18%	0.20%	−17%
	50	0.09%	−47%	0.15%	−50%
	60	0.07%	−56%	0.12%	−54%

Fluidity was increased through water addition, since no effective plasticizer agent has been found yet for this family of geopolymers [36]. This addition has two main shortcomings. First of all, water increases porosity and, thus, reduces both compressive and tensile strength, hindering the capability of counteracting stresses induced by drying shrinkage. Secondly, high fluidities may induce or facilitate the segregation of aggregates, since coarser fractions tend to sink and fines tend to emerge.

The investigation started from mixtures, containing mixed waste aggregates MX1, made with a K-silicate activator with molar modulus K_2O/Si_2O of 2.3 and dry matter concentration of 42%. The reference mixtures had a molar ratio K/Al of either 0.66 (FL-A) or 0.55 (Flfa-A, with 9% dw of fly ash). Those mixtures, without or with fly ash, were set to have a rather low viscosity, approximately smaller than 1000 Pa·s, but retaining a thixotropic behaviour. Then, fluidity was increased to obtain mixtures able to be poured by gravity. The reduction of viscosity was achieved in two manners: by increasing the amount of extra water added during mixing (FL-B and FLfa-B), or by increasing the amount of alkali activator to equate the quantity of extra water through solvated water contained in the K-silicate solution (FL-E, FLfa-C and FLfa-D), increasing in this manner also the K/Al ratio. FL-F was prepared with a K-silicate with molar modulus SiO_2/K_2O of 1.4 and dry matter concentration of 45%, and had a K/Al of 0.84. Two additional mixtures with larger amounts of extra water, and no fly ash, were tested as well (FL-C and FL-D).

Fig. 3 compares the performance in terms of compressive strength and initial viscosity. As a reference, the range of suitable initial viscosity at ordinary room temperatures (20–23 °C) of mixtures formerly studied [36] was found in the range 1000–2000 Pa·s. Viscosities approximately lower than 800 Pa·s rendered the mixture able to flow by gravity. Values in the range 80–100 Pa·s implied a 28-day strength range of about 32–50 MPa. The overall best performance in terms of fluidity and strength was provided by mixtures with exceeding K-silicate activator. As a probable consequence of the curing temperature of 50 °C, the amount of shrinkage measured on cylindrical specimens was kept approximately in the range 0.10–0.15% during the first 5 weeks.

A minimum open time of approximately 1 h, empirically evaluated on small samples at room temperatures of about 20 °C, was observed in all cases. The addition of fly ash, combined with the adopted alkaline activator, had a clear beneficial effect, leading to mixtures workable for hours.

Unfortunately, the encouraging results in terms of fluidity, strength and open time were hindered by issues observed in real-scale prototypes, mostly related to cracking and excessive differential deformations due to drying shrinkage. Apparent differential deformations were observed also in specimens whose desiccation was rather uniform: this was imputed to excessive segregation of aggregates during casting, due to pouring and vibration. Indeed, a preliminary investigation on mixtures with either concrete or fired clay aggregates cured at 30 °C (details about composition and strength can be found in the previous work [36]) highlighted a drying shrinkage remarkably greater in mixtures with predominant fractions of fine aggregates, compared to mixtures with mostly coarser aggregates (Fig. 4). The difference was approximately comprised between 30% (concrete aggregates) and 40% (fired clay aggregates) in the first 2 days, and between 30% (fired clay aggregates) and almost 70% (concrete aggregates) after about 1 year.

Consequently, further countermeasures against the effects of drying shrinkage were taken, namely: reduction of water content to reduce slightly the fluidity and limit the segregation of aggregates; increase of the content of potassium to improve the strength; modification of the particle size distribution of recycled aggregates. In particular, two types of recycled sand were produced by screening MX1 during production, one (MXf) with about 83% by weight of particles below 1 mm, the second (MXc) with about 90%

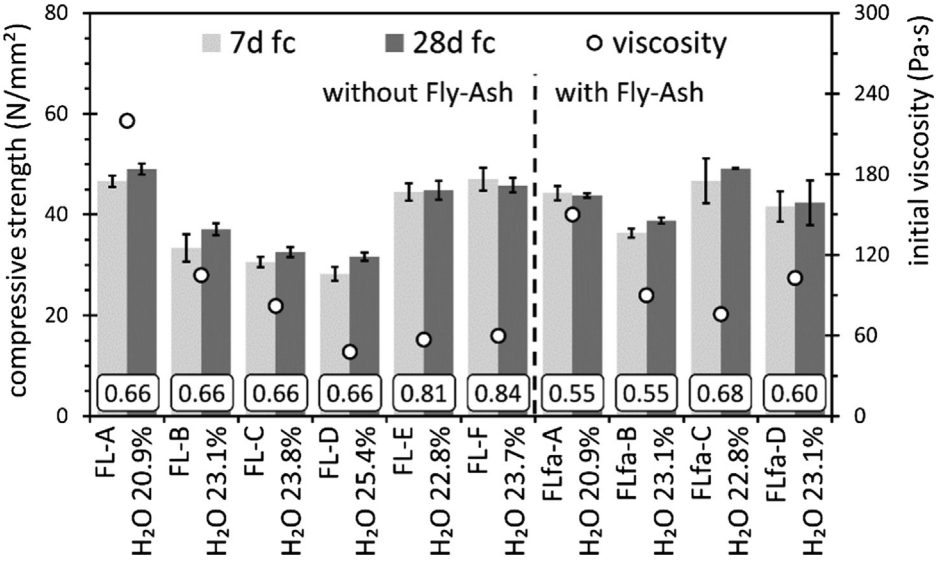

Fig. 3. Pourable mixtures compared in terms of compressive strength (error bars represent ±1 standard deviation) and initial viscosity. The K/Al molar ratio is reported inside frames, indicating an addition of extra water or an increased amount of K-silicate activator.

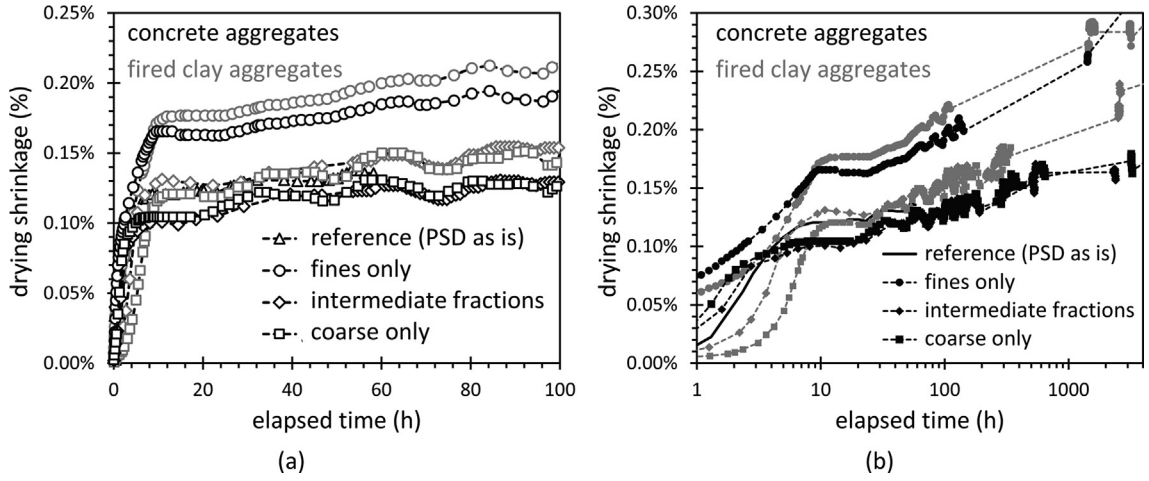

Fig. 4. Effect of particle size distribution on shrinkage: (a) first 100 h and (b) up to 6 months.

between 1 and 2 mm. This separation was supposed effective also in reducing segregation problems during transportation and storage of the aggregates.

3.2.1. Influence of type of metakaolin and commercial silicate activator.

Since metakaolin MK0, used at first, was not commercially available anymore, it was replaced by MK1. As expected, the coarser granulometry of MK1 determined a lower reactivity in the geopolymer mix, reflected by a loss of strength of identical mixtures prepared with either MK0 or MK1 (Fig. 5). Two recipes with mixed waste MX1, i.e. FL-B and FLfa-B, were compared, the latter including 9% dry weight of class F fly ash FA0. Results indicated a decrease of compressive strength comprised between 14% and 23% at 7 days, reduced to about 8% at 28°days, with a relative increase in porosity of about 5% for both recipes.

A possible influence of the industrial process for the preparation of K-silicate activators was also investigated by comparing the strength of identical mixtures, one with sand aggregates (Ksd) and the second with waste aggregates (Kwa), prepared with MK1 and with either an in-house prepared K-silicate or a commercial

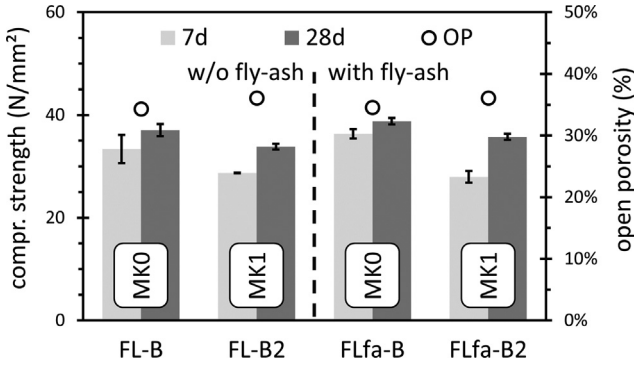

Fig. 5. Comparison of mixtures with MK0 or MK1 in terms of compressive strength (±1 standard deviation) and open porosity (secondary y-axis).

product that reproduced the same formulation. Indeed, the use of the same industrial reactors for producing both Na-silicates and K-silicates can determine a presence of Na_2O, which is known to deliver materials with a strength generally lower than K-silicates

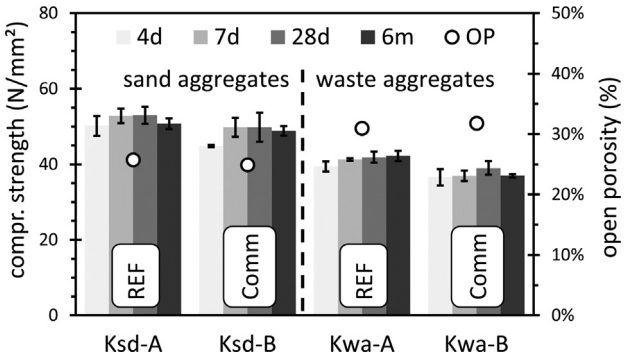

Fig. 6. Comparison of in-house made (REF) and commercial K-silicate activators in terms of compressive strength (±1 standard deviation) and open porosity (secondary y-axis).

[46], also in potassium silicates, being the accepted allowance generally comprised between 1% and 4%. Results (Fig. 6) indicated a slight loss of strength for mixtures with the commercial activator, about 6–7% at 28 days, which changed to 4% in case of sand aggregates and to 12% for waste aggregates at 6 months.

4. Features of the final materials

4.1. Mechanical and physical characterization

The final recipe (FG) was based on the outcomes of preliminary tests reported in Panizza et al [36] and of further investigations described above. Results of laboratory tests were heuristically combined with observations of prototype panels manufactured in parallel. Ingredients are listed in Table 4, referred to the overall dry weight (i.e. detracted the water contained in the alkali activator). The fresh mixture, at about 23 °C, presented a viscosity in the range 120–150 Pa·s, an open time greater than 70 min, measured from the beginning of the reaction and estimated through the increase rate of viscosity (after 75 min it was approximately twice, and it reached 1000 Pa·s after about 90 min), and a density of about 2.1 g/cm^3.

At first, the two available recycled sands, namely MXf (fine particles below 1 mm) and MXc (coarser aggregates between 1 and 2 mm) were blended in 2:3 proportion (mixtures FG1), a ratio that was subsequently changed into 1:2 (mixtures FG2) to reduce the amount of fines for improving workability. The effects of this little modification (see Fig. 1) on the properties of the hardened material were however negligible, as can be seen in Table 5 and Table 6, which report the measured physical and mechanical properties, respectively. For the sake of completeness, Table 6 presents also the characteristic values of strength (i.e. 5-percentile), which is a typical design quantity in Civil Engineering, calculated according to the Eurocode 0 approach assuming unknown variance (use of a central t-Student distribution) [47]. The matrix alone (MTX), i.e. the geopolymer paste without aggregates, was tested as well, although it might not represent perfectly the matrix when aggregates are included, due to a possible absorption of the liquid phase by the waste that might induce variations in ratio of components and water content.

Bending tests were carried out on 6 specimens of mixture FG2, delivering a strength f_b of 5.9 N/mm^2 (CoV 7.3%) and a bending vs splitting strength ratio f_b/f_{sp} of 1.79. As a term of comparison, available data on 16 mixtures with different features provided f_b/f_{sp} ratios comprised in the range 1.35–1.85, with an average of 1.64 (CoV 8.6%). Six prismatic specimens with square cross section 22 × 22 mm^2 and height 44 mm, from a batch of mixture FG2, were tested in compression at 28 days of age. Incidentally, they delivered an average strength f_c of 38.1 N/mm^2, in line with the overall mean of cylindrical specimens, but 5% lower than a set of 6 cylinders coming from the same batch and tested in parallel. The difference might be due to a slightly more challenging preparation of the surfaces, or might be geometry dependent to some extent, as formerly conjectured by van Mier et al [48].

Reference specimens were used as a term of comparison for drying shrinkage. Three materials, cured at ambient temperature, were selected, namely a category M15 [49] pre-mixed cement-free pozzolana lime mortar with siliceous sand aggregates (LM prepared with 24% by weight of water according to its technical datasheet, average 28-day f_c of 18.0 N/mm^2, open porosity of 34.1%), an improved cementitious adhesive for tiling (CA prepared with 30% by weight of water according to its technical datasheet, average 28-day f_c of 23.6 N/mm^2, open porosity of 41.9%), and a Portland cement mortar with fine siliceous sand made with a water:cement ratio of 0.30 and a cement:sand ratio of 1.4 (other properties not available). Results are shown in Fig. 7a (first 48 h) and 7b (up to 5 weeks). After two weeks, the shrinkage of FG mixtures was comprised between 0.14% and 0.16%, while that of the matrix alone (MTX) was remarkable as expected (about 0.46%), the cementitious mortars CM reached 0.16%, the lime mortar LM and the cementitious adhesive CA approached 0.23% and 0.31%, respectively. LM reached 0.35% after 10 weeks, while the shrinkage of an FG specimen did not exceed 0.22% after 6 months. Interestingly, conditions kept constant, all the geopolymer mixtures tested so far showed a distinctive behaviour compared to reference materials, which consisted in a steep increase of shrinkage in the first 8–12 h, followed by a rather horizontal branch and a subsequent slower progression. In addition, geopolymers appeared more sensitive to daily variations of air relative humidity, as indicated by shrinkage/swelling fluctuations

Table 4
Composition of the final geopolymeric mixtures referred to the dry weight (K-silicate includes water).

Ingredients	MK	SL	FA	K-silicate	Aggregates	PP fibres	Water content
Quantity (% dry weight)	17.8%	11.9%	5.9%	36.1%	48.2%	0.15%	19.9%

Table 5
Average physical properties of final mixtures and matrix (coefficient of variation in brackets).

Mixture	6-month ρ_{ap} kg/m^3	ρ_b kg/m^3	ρ_m kg/m^3	*OP* %	*WA* %
FG1*	$1.89{\cdot}10^3$ (1.3%)	$1.78{\cdot}10^3$ (2.3%)	$2.53{\cdot}10^3$ (0.8%)	29.7% (4.2%)	16.7% (6.3%)
FG2*	$1.89{\cdot}10^3$ (0.9%)	$1.77{\cdot}10^3$ (1.1%)	$2.51{\cdot}10^3$ (1.0%)	29.8% (3.1%)	16.8% (3.9%)
MTX†	$1.61{\cdot}10^3$ (0.3%)	$1.40{\cdot}10^3$ (1.1%)	$2.44{\cdot}10^3$ (1.6%)	42.6% (1.2%)	30.4% (1.2%)

* At least 9 specimens in overall, from at least 3 batches.
† 6 specimens from 2 batches.

Table 6
Average (avg) and characteristic (5-percentile – chr) mechanical properties of final mixtures and matrix (coefficient of variation in brackets).

Mixture		Compressive strength f_c (N/mm^2)						Splitting strength f_{sp} (N/mm^2)					
		7-day		28-day		6-month		7-day		28-day		6-month	
FG1*	avg	43.0	(5.2%)	37.4	(6.8%)	37.7	(3.5%)	3.49	(6.3%)	3.09	(11.5%)	3.21	(12.0%)
	chr	38.8		32.8		35.1		3.07		2.41		2.45	
FG2*	avg	40.9	(4.2%)	37.7	(5.8%)	38.5	(4.6%)	3.21	(7.4%)	3.27	(7.6%)	3.25	(12.4%)
	chr	37.5		33.8		34.9		2.74		2.77		2.45	
MTX†	avg	39.6	(3.1%)	26.4	(5.4%)	25.5	(5.1%)	2.17	(12.4%)	2.54	(2.1%)	2.27	(3.9%)
	chr	35.4		21.6		21.1		1.27		2.37		1.97	

* At least 8 specimens in overall, from at least 2 batches.
† 3 specimens from a single batch.

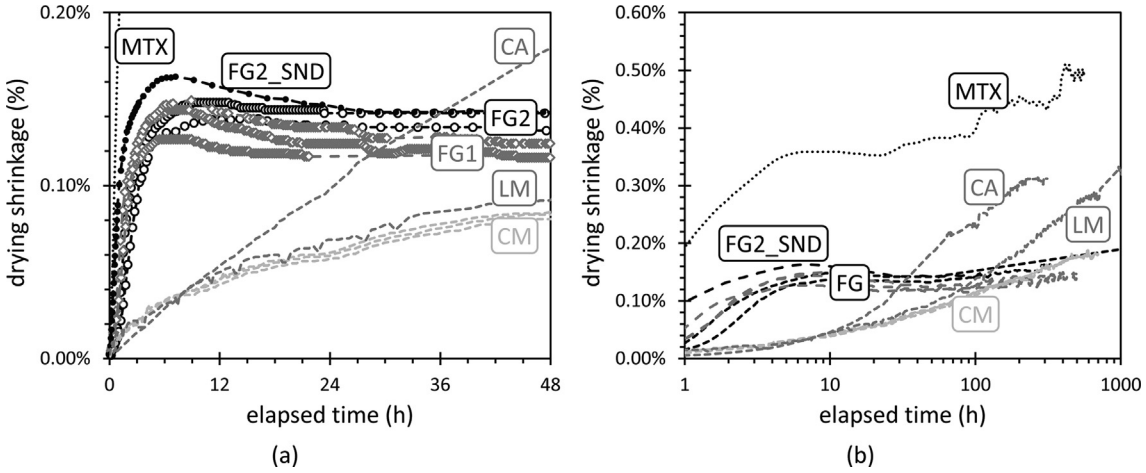

Fig. 7. Drying shrinkage of final mixtures, compared to reference materials: (a) first 2 days and (b) up to 5 weeks.

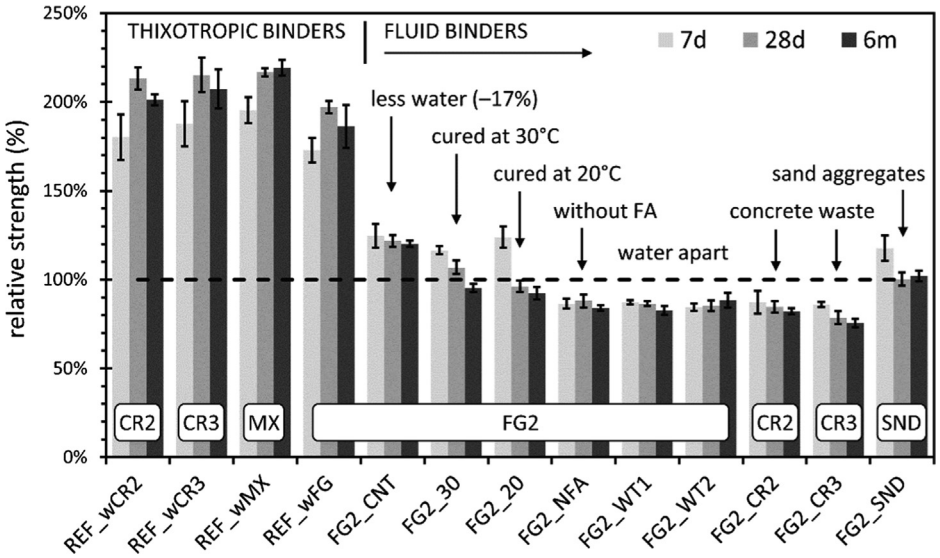

Fig. 8. Comparison of compressive strengths related to variations of binder, aggregates and curing conditions, normalized to the corresponding strength of FG2 mixtures tested at the same age. The type of aggregate is indicated inside a frame. Error bars represent ±1 standard deviation.

(the possible contribution due to temperature variations was reasonably negligible compared to humidity). However, no explanation can be herein provided, owing to the complex mechanisms of geopolymer shrinkage not yet clarified, which would require dedicated investigations. Nonetheless, the different role of water, compared to hydrated cementitious materials, is to be mentioned [45].

4.2. Comparisons and long term behaviour

The compressive strength of final mixtures was compared to reference thixotropic ones, and parameters such as temperature of curing, type of aggregate, and water content, were varied to measure their effect on the mechanical performance (Fig. 8 and Table 7).

Table 7
Evolution of compressive strength in the short and long term, normalized to the corresponding 28-day value. The notation "b" followed by a number indicates different batches of the same material.

Mixture	28-day strength		Normalized strength (standard deviation in brackets)									
	N/mm^2	CoV	3-day		7-day		3-month		6-month		1-year	
REF_wCR2	80.35	2.9%	–		0.92	(0.07)	1.03	(0.05)	0.96	(0.02)	–	
REF_wCR3	81.05	4.5%	–		0.95	(0.06)	0.95	(0.01)	0.98	(0.05)	–	
REF_wMX	81.66	1.0%	–		0.98	(0.04)	–		1.03	(0.02)	–	
REF_wFG	74.28	1.8%	0.93	(0.01)	0.95	(0.04)	–		0.97	(0.06)	–	
FG2_CNT	45.86	2.8%	1.25	(0.07)	1.11	(0.06)	1.02	(0.01)	1.01	(0.01)	–	
FG2_30	40.25	3.6%	1.11	(0.02)	1.18	(0.02)	–		0.91	(0.02)	–	
FG2_20	36.26	3.4%	–		1.40	(0.07)	–		0.98	(0.04)	–	
FG2_NFA	33.18	4.2%	–		1.07	(0.03)	0.92	(0.02)	0.97	(0.02)	–	
FG2_WT1	32.59	1.7%	1.22	(0.06)	1.10	(0.01)	1.02	(0.04)	0.98	(0.03)	–	
FG2_WT2	32.12	3.5%	1.28	(0.05)	1.07	(0.02)	1.14	(0.03)	1.06	(0.05)	–	
FG2_CR2	31.91	3.8%	1.28	(0.04)	1.12	(0.08)	1.01	(0.04)	0.99	(0.02)	–	
FG2_CR3	29.63	4.6%	1.36	(0.07)	1.19	(0.02)	1.03	(0.01)	0.98	(0.03)	–	
FG2_SND_b1	38.65	3.8%	–		1.30	(0.04)	–		1.04	(0.02)	–	
FG2_SND_b2	36.88	1.7%	1.23	(0.04)	1.24	(0.04)	–		1.04	(0.00)	–	
FG1_b1	36.49	1.4%	–		1.14	(0.03)	–		1.04	(0.02)	1.04	(0.04)
FG1_b2	38.76	2.5%	1.29	(0.06)	1.15	(0.04)	0.93	(0.04)	1.00	(0.01)	0.95	(0.03)
FG1_NFB	33.56	2.2%	–		1.31	(0.09)	–		1.08	(0.03)	–	
FG2_b1	36.28	4.7%	1.21	(0.05)	1.11	(0.03)	1.04	(0.08)	1.08	(0.04)	1.10	(0.03)
FG2_b2	35.79	0.6%	1.14	(0.09)	1.16	(0.07)	–		1.05	(0.06)	–	

The reference thixotropic binder (Si/Al ≈ 2.3, K/Al ≈ 0.75, water content ≈ 16.6%, nominal aggregate content ≈ 50%), which was among those presented in Panizza et al. [36], was replicated with concrete waste CR2 and CR3 (mixtures REF_wCR2/3), delivering results consistent with those previously reported [36] and demonstrating a scarce sensitivity to the type of input waste concrete, being the strength at 28 days about 80 N/mm^2 for all of them. Mixture REF_wMX was made with the same recipe but with one half of concrete CR1 and one half of fired clay FC1 waste aggregates, and suggested that the presence of fired clay generally improves the mechanical behaviour, probably owing to a partial reactivity greater than concrete, despite the extra water required to achieve a similar workability (water content ≈ 17.6%), as already observed [36]. Then, mixed waste aggregates MXf and MXc, with PSD as in FG2, were used in REF_wFG2 (water content ≈ 16.4%), resulting in a loss of strength of about 10–15%, compared to REF_wMX, that might be attributed to the different PSD.

The pourable binder (Si/Al ≈ 2.2, K/Al ≈ 0.80, water content ≈ 19.9%) was subsequently subjected to several variations to test its robustness. Firstly (FC2_CNT), the water content was reduced from 19.9% to 16.4% (same as REF mixtures) by using a sample of K-silicate with solid matter concentration of 50% instead of 45%, resulting in a strength increase of about 20% compared to FG2, but showing a loss of about 35% compared to REF_wFG that should be due to the different binder composition. Then, the 12-hour initial curing temperature was lowered from 50 °C to 30 °C (FG2_30) and 20 °C (FG2_20), with a performance in the long term substantially similar to FG2. Fly ash was replaced in mixture FG2_NFA by furnace slag (Si/Al ≈ 2.3, K_2O/Al_2O_3 ≈ 0.88), bringing back the MK:SL ratio to 1:1 used in previous researches, showing that the presence of fly ash was not detrimental to the strength. Mixtures FG2_WT1 and FG2_WT2 were made with the same concentrated activator of FG2_CNT, but the water content was restored to 19.9% by adding extra water either directly in the binder paste, before the introduction of waste aggregates (FG2_WT1), or soaking the aggregates in advance (FG2_WT2); the outcomes suggested that the use of solvated water coming only from the alkali activator might be more effective from a mechanical standpoint. Concrete waste aggregates CR2 and CR3 were embedded in FG2_CR2 and FG2_CR3, resulting in a strength loss of about 20% compared to FG2, and providing another indication that the presence of fired clay might have a beneficial effect on the strength. In addition, the loss of strength compared to REF_CR2/3, about 60%, was roughly comparable to that observed between REF_wMX and FG2. Finally, FG2_SND was prepared with fine siliceous sand, showing no remarkable difference in the long term.

The 28-day compressive strength and the evolution in the short and long term up to 6 months, normalized to the corresponding 28-day value, are reported in detail in Table 7 for the previous mixtures, for two batches of FG1, one batch of FG1 without short fibres (FG1_NFB, whose performance was substantially similar to parent mixtures) and two batches of FG2. Apart from an unexpected gain of strength during the first days exhibited by pourable binders, which is still under investigation and seemed to be unexpectedly enhanced by lower curing temperatures, results confirmed a fair stability in the long term. Ratios of compressive strength, measured from 3 months onward, to that measured at 28 days, despite an expected scatter, delivered a mean value of 1.01 (1.03 for the three mixtures tested at 1 year), suggesting that 28 days can be reasonably assumed as a reference age also for these family of geopolymer materials, similarly to concrete and mortar.

5. Geometry of test specimens in compression

With a maximum nominal aggregate size of 2 mm, these materials might be assimilated to mortars. Nonetheless, standard prism specimens 40 × 40 × 160 mm^3 complying with EN 1015-11 [50] were not used for compressive tests, but cylinders with diameter of 22 mm and height-to-diameter ratio of 2, whose volume is approximately 1/15 of mortar standard prisms, were adopted instead [36]. Indeed, the extensiveness of previous and ongoing researches would have required about 3 ton of materials instead of about 200 kg if standard prisms were used. In addition, the thickness of panels under development was comprised between 6 and 30 mm, thus close to the specimen size.

5.1. Aspect ratio

To highlight how this family of geopolymeric mixtures stands toward the current knowledge of concrete and rock materials, the aspect ratio of specimens with diameter 22 mm (Fig. 9a) was investigated in the range 0.25–3 (one batch of mixture FG1) and 0.5–3 (one batch of mixture FG2), tested at 28 days with 3 repeti-

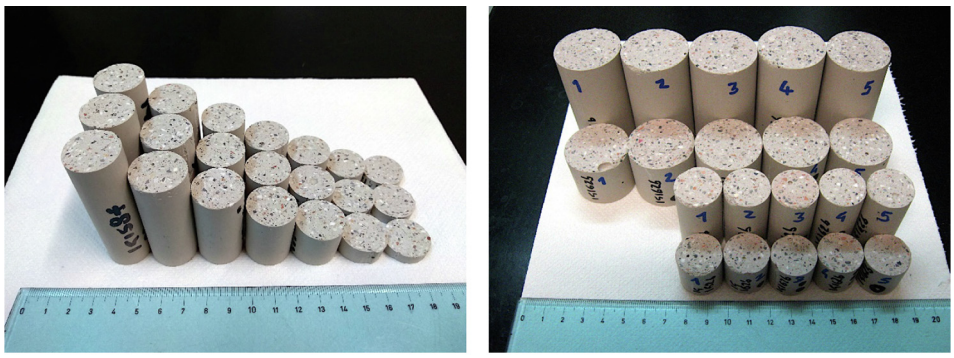

Fig. 9. A set of specimens for investigating in compression the aspect ratio (a) and a set for 22 mm vs 35 mm diameters (b).

tions for each value. Specimens with diameter 35 mm were investigated as well (Fig. 9b), with aspect ratio of either 2 or 1 to derive a direct comparison of cylindrical and cubic compressive strength, using a batch of mixture FG1 and one of FG2, tested at 2 months (5 repetitions for each configuration) and 10 months (4 repetitions).

The aspect ratio and the diameter of compression specimens is a topic mostly investigated in the case of concrete cores, being a widely accepted method of determining the strength in existing structures or pavements [51–55], and cores of intact rock materials [56–59]. Generally, concrete cores should have a diameter of 100–150 mm, which if often impracticable on-site, therefore the use of small (45–50 mm) and micro (28 mm) core sizes have been investigated [52–55], although results are affected by the ratio of diameter and maximum aggregate size that can approach values even lower than 2, in case of smaller cores. For rock materials, a diameter of 50 mm is generally regarded as a reference size, with a minimum length-to-diameter ratio of 2 [56–59].

Fig. 10 shows the measured relative strengths (i.e. divided by the average strength of the corresponding set of specimens with diameter D of 22 mm and height H of 44 mm) as a function of the H/D ratio. Data included two geopolymeric recipes, FG1 and FG2, and a pre-mixed cementitious grout for injections without aggregates (CG, specimens with diameter 22 mm) prepared with a water/binder ratio of 0.32, tested for comparison.

Two predictive curves for concrete (no analytical expression available) provided by the US Bureau of Reclamation [60] (USBR 1992) and Neville [61] (Neville 2010), which are indeed very close, and a curve (Eq. (8a), where $f_{c,ref}$ is the reference compressive strength for an aspect ratio of 2 and f_c is the compressive strength measured at D/H) proposed for rocks [56] (Turk 1986), which averages the coefficients of three previous correlations, were superimposed to test results in Fig. 10a. It can be noted that, for aspect ratios lower than 1, the curve for rock materials is apparently closer to the experimental data than the curves for concrete. This might be explained by the greater ratio of specimen height and maximum aggregate size in the case of the tested geopolymers, which was still greater than 5 for H/D of 0.5, while in the case of concrete cores with diameter 100 mm it can easily approach 2 or less. Indeed, the aggregate size is supposed to affect also aspects like tensile strength and fracture energy of inorganic composite materials, as known for cement concrete and mortar [62].

Fig. 10b shows the results of two non-linear least squares fitting, carried out separately on geopolymeric specimens with a diameter of 22 mm (77 data points, FC1 + FC2) and cementitious grout specimens (31 data points, CG), the first (FitA, Eq. (8b)) corresponding to Eq. (8a) recast, the second (FitB, Eq. (8c)) differing in the aspect ratio raised to the square. Parameters were obtained by a numerical minimization of the residual sum of squares (*RSS*, Eq. (9a) where y are the measured values and $\hat{y}$ the calculated values) via a commercial spreadsheet software and an open-source software for numerical computation (Scilab 6.0.1 [63]), which practically delivered the same values. Results are reported in Table 8, together with the coefficient of determination R^2 (Eq. (9b) where $\bar{y}$ is the sample mean of y), corresponding to R_1^2 discussed by Kvalseth [64], and the Root Mean Square Error (*RMSE*, Eq. (9c) where N

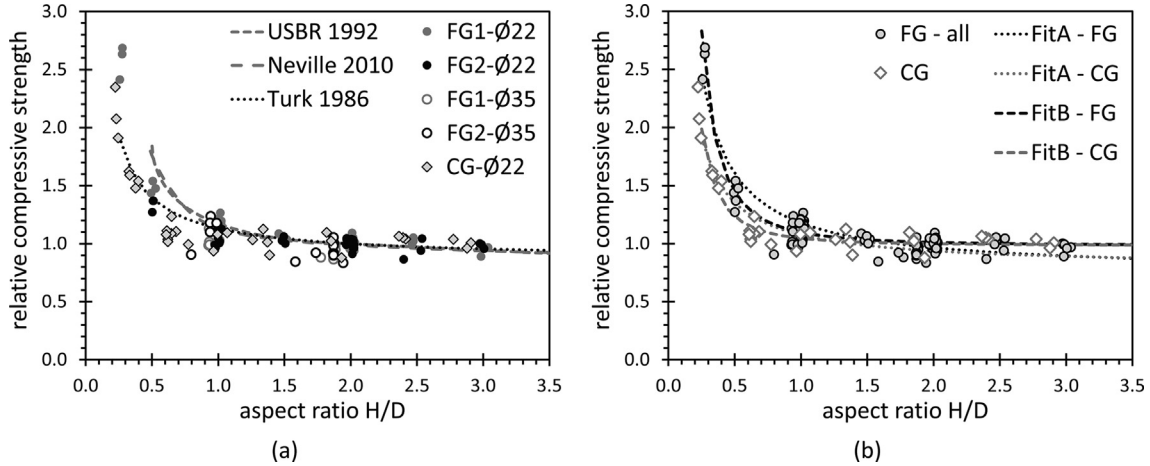

Fig. 10. Experimental data plotted against the available predictive curves for concrete and rocks (a) and against the calculated regression curves (b).

Table 8
Results of the least squares fitting, with coefficient of determination (R^2) and Root Mean Square Error (RMSE).

	FitA		FitB		Neville 2010		Turk 1986	
	FC1 + FC2	CG	FC1 + FC2	CG	FC1 + FC2	CG	FC1 + FC2	CG
A	0.753	0.800	0.982	0.983	–	–	–	–
B	0.424	0.276	0.115	0.063	–	–	–	–
R^2	0.883	0.874	0.944	0.948	0.866	< 0	0.751	0.852
RMSE	0.109	0.125	0.075	0.081	0.279	0.440	0.181	0.285

is the number of observations). The performance of predictive curves Neville 2010 (approximated via an 8th grade polynomial function, with $R^2 > 0.999$) and Turk 1986 are reported for comparison. It can be noted that FitB curves ($R^2 > 0.94$, $RMSE \approx 0.08$) depict the experimental data better than FitA, while the available prediction curves Neville 2010 and Turk 1986 present a satisfactory R^2 (except in one case) but a greater *RMSE*, not smaller than 0.28 and 0.18, respectively.

$$\text{(a) } \frac{f_{c,ref}}{f_c} = \frac{1}{0.86766 + 0.26466 \cdot (D/H)} \quad \text{(b) } \frac{f_c}{f_{c,ref}} = A + \frac{B}{(H/D)} \quad \text{(c) } \frac{f_c}{f_{c,ref}} = A + \frac{B}{(H/D)^2} \tag{8}$$

$$\text{(a) } RSS = \sum \left(y - \hat{y}\right)^2 \quad \text{(b) } R^2 = 1 - \frac{RSS}{\sum (y - \bar{y})^2} \quad \text{(c) } RMSE = \sqrt{\frac{RSS}{N}} \tag{9}$$

5.2. Diameter size

Regarding the comparison between the two diameters tested in compression, it is worth pointing out that the investigation was not aimed at depicting the size effect, which can be reasonably assumed to exist [65,66], since it would require a dedicated experimentation involving a significantly larger size range. The strength ratio of samples with diameter 35 mm and 22 mm for the two mixtures tested at 2 and 10 months of age was comprised between 0.90 and 0.99, with a mean of 0.93. It is worth noting that the preparation of larger specimens was more challenging in terms of smoothness and planarity of surfaces, and the size might have intensified possible unevenness of loading. Nonetheless, without entering the entangled aspects of deterministic and statistical size effects in fracture mechanics, and relying only on empirical observations, data of different geometries were compared in terms of relative strength (i.e. divided by the average strength $f_{c,Dref}$ related to the reference diameter D_{ref} of 22 mm) as per Eq. (10b) (where n is an empirical constant), which correspond to Eq. (10a) recast that was proposed [56] to standardize the uniaxial compressive strength of rock specimens to that of 50 mm diameter specimens, and per Eq. (10c) (where V_i is the specimen volume and m is the Weibull's modulus), which is based on Weibull's statistical theory of strength. The latter has been frequently applied also to laboratory size specimens of quasi-brittle materials, despite criticism [67], recently also in the case of cylindrical test samples made of autoclaved aerated concrete for masonry units [68].

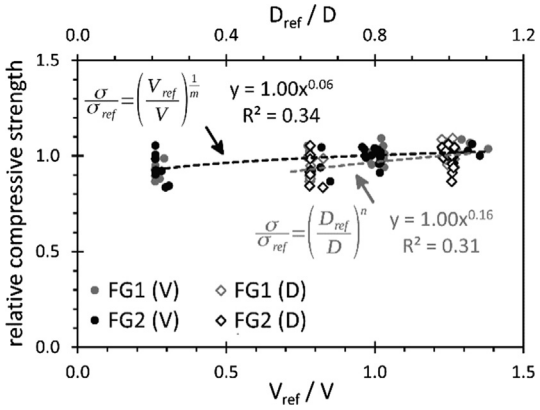

Fig. 11. Relative strength values plotted against diameter ratio (grey markers and trend line) and volume ratio.

Interestingly (Fig. 11), despite the relevant scatter of data points that affected the R^2 of trend lines, regression curves delivered in both cases a multiplicative coefficient (1.003 for both regressions) equal to 1 up to three significant figures, and a reasonable value of the exponent, i.e. 0.163 for the variation of the diameter and 0.058 (which corresponds to $m \approx 17$) for the variation of the volume. In the case of Eq. (10b), values between 0.18 and 0.22 can be found for rocks [59], while for mortar and concrete a range of m between 12 and 24 has been reported [67]. By extrapolation, these empirical regressions, which provide similar outcomes, might allow a rough estimate of the expected average strength for larger test specimens based on 22 mm diameter.

$$\text{(a) } \frac{f_{c,50}}{f_c} = \left(\frac{D}{50\text{ mm}}\right)^{0.18} \quad \text{(b) } \frac{f_c}{f_{c,Dref}} = \left(\frac{D_{ref}}{D}\right)^n \quad \text{(c) } \frac{f_{c,1}}{f_{c,2}} = \left(\frac{V_2}{V_1}\right)^{\frac{1}{m}} \tag{10}$$

5.3. Cube versus cylinder compressive strength

Finally, the ratio between the assumed "cylinder" (aspect ratio of 2:1) and "cube" (aspect ratio of 1:1) compressive strength was calculated for both diameters (i.e. 22 mm and 35 mm). Results (Table 9), taken individually, show a certain scatter and no particular correlation with diameter or age of testing. Nonetheless, their values comprised between 83% and 96% (89% in average) are in line with expectations, since in literature and standards similar ranges can be found for high-friction boundary conditions of concrete specimens, which are the most common [69]. For example, Meininger et al. [51] reported 0.84–0.90 for dried specimens and

Table 9
Measured cylinder vs cubic strength ratios.

Mixture	FG1_b3-HD	FG1_b4-DM		FG2_b4-HD	FG2_b5-DM		Overall mean
Diameter	22 mm	22 mm	35 mm	22 mm	22 mm	35 mm	
28 days	83.2%	–	–	95.3%	–	–	89.2% ± 5.1%
2 months	–	89.1%	92.7%	–	95.8%	84.5%	
10 months	–	83.8%	–	–	89.5%	–	

0.85–0.90 in average, 0.78–0.89 for concrete cores and 0.85–0.87 for cylindrical specimens, based on previous works; many found a dependence on strength, e.g. the Model Code 2010 [70] provides values between 0.80 and 0.86 for concrete classes C12–C120, and between 0.89 and 0.92 for lightweight concrete classes LC8–LC80, while Parsekian et al. [71], in the case of mortar prism halves and cylinder specimens, found values close or even greater than 1 for the strongest mixes. It is worth mentioning that, for a given aspect ratio, prismatic and cylindrical specimens are generally considered equivalent despite the different cross-sectional geometry, but a different behaviour would not be unexpected, although not clearly explained [48].

6. Splitting versus compressive strength

The splitting strength f_{sp}, which is incorporated in most concrete design codes through Eq. (2) [72], owing to its relatively simple determination, was assumed to be a fairly reliable indicator of the uniaxial tensile strength of the investigated geopolymers, although it cannot be considered as a material property. Albeit it is known that the measured values depend upon several aspects, among them geometry and size of specimens, and relative width of the load-bearing strips [72], the adoption of cylindrical specimens without packing strips, having a diameter/aggregate size ratio greater than 10, was assumed to mitigate the dependence of results from the above mentioned factors and the deviation from the elastic interpretation. In addition, the low amount of short fibres, if present, did not appear to affect the first crack load, which was used for the computation of strength. Concerning the relation between splitting and uniaxial tensile strength, according to the Model Code 2010 [70], existing codes and standards for concrete generally provide a conversion factor α_{sp} that may vary from 0.67 to 0.95, although recent researches suggest values beyond 1. Indeed, the Model Code 2010 [70] proposes 1.0 as a compromise.

This section reports data of 99 (at 7 days of age) and 130 (at 28 days) geopolymer mixtures tested so far in previous [36] and ongoing researches, having molar ratios Si/Al between 1.8 and 2.4 (sets tested at 7 days) and 1.8–2.6 (sets tested at 28 days), K/Al between 0.49 and 0.98 (7 days) and 0.49–1.14 (28 days), and water contents between 15% and 27%.

As previously noted [36], most splitting-to-compressive strength ratios are comprised in the range 5–10%, with greater values for lower compressive strengths (Fig. 12). Although the average splitting-to-compressive strength ratio measured at 28 days of age was about 7% regardless the aggregate type, an empirical power law regression (Eq. 11a) appears to describe satisfactorily the observed trends. Results at 7 days of age (Fig. 12a) were apparently less dispersed than those observed at 28 days (Fig. 12b), as a probable consequence of the different variation of compressive and splitting strength with time.

Least square fitting curves (Eq. (11a), where C_1 and C_2 are regression constants), calculated through regression lines on natural logarithms of data points grouped into mixtures with waste aggregates (81 and 110 points at 7 and 28 days, respectively) and natural sand aggregates (18 and 20 points), are shown in Fig. 13a and 13b for results at 7 and 28 days of age, respectively. The function proposed for concrete by the Model Code 2010 [70], reported in Eq. (11b) (where f_{ctm} is the mean tensile strength, Δf is 8 N/mm^2, $f_c - \Delta f$ replaced the original f_{ck}, i.e. the characteristic compressive strength, and C50 is the class of concrete with f_{ck} of 50 N/mm^2), was superimposed for comparison to the experimental data. Numerical results of the fitting are listed in Table 10, together with the relative R^2 and *RMSE* (see Section 5), calculated also separately for each waste (concrete: 23 and 29 points at 7 and 28 days, respectively; fired clay: 19 and 26 points; mixed aggregates: 33 and 49 points), not considering 6 mixtures with either recycled geopolymer or glass waste aggregates included in the overall regressions. In all cases, the greatest value of R^2 and the lowest *RMSE* were obtained for mixtures with mixed waste aggregates. Nonetheless, the fitting of all waste and siliceous sand aggregates described satisfactorily the experimental data ($R^2 \geq 0.80$ ca, RMSE < 0.45 ca), while the Model Code 2010 [70] delivered acceptable results at 28 days of age, except for siliceous sand aggregates. Data on geopolymer concrete retrieved from literature were superimposed in Fig. 13b for comparison. They relate to three works involving class F fly ash based geopolymers activated by NaOH and Na-silicate solutions, tested by means of 100 × 200 mm^2 and 150 × 300 mm^2 cylinder specimens. Coarse aggregates were either crushed basalt with maximum size 14 mm [73], crushed rock with maximum size 19 mm [74], or crushed granite between 7 and 20 mm [75].

$$\text{(a)}\ f_{sp} = C_1 \cdot f_c^{C_2}$$

$$\text{(b)}\ \begin{cases} f_{ctm} = 0.3 \cdot (f_c - \Delta f)^{2/3} & \text{concrete grades} \leq \text{C50} \\ f_{ctm} = 2.12 \cdot \ln(1 + 0.1 \cdot f_c) & \text{concrete grades} > \text{C50} \end{cases} \quad (11)$$

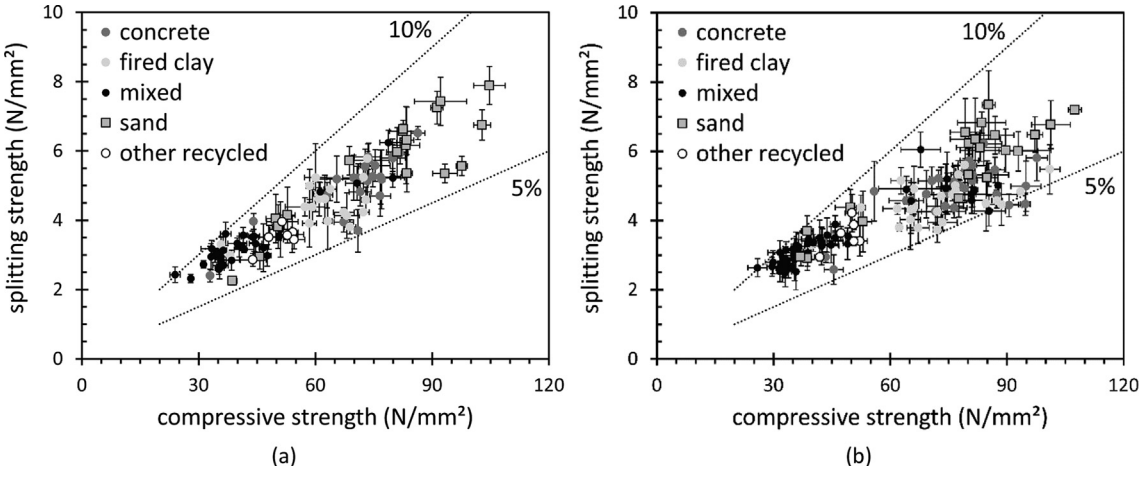

Fig. 12. Splitting versus compressive strength at 7 days (a) and 28 days (b). Error bars represent ± 1 standard deviation.

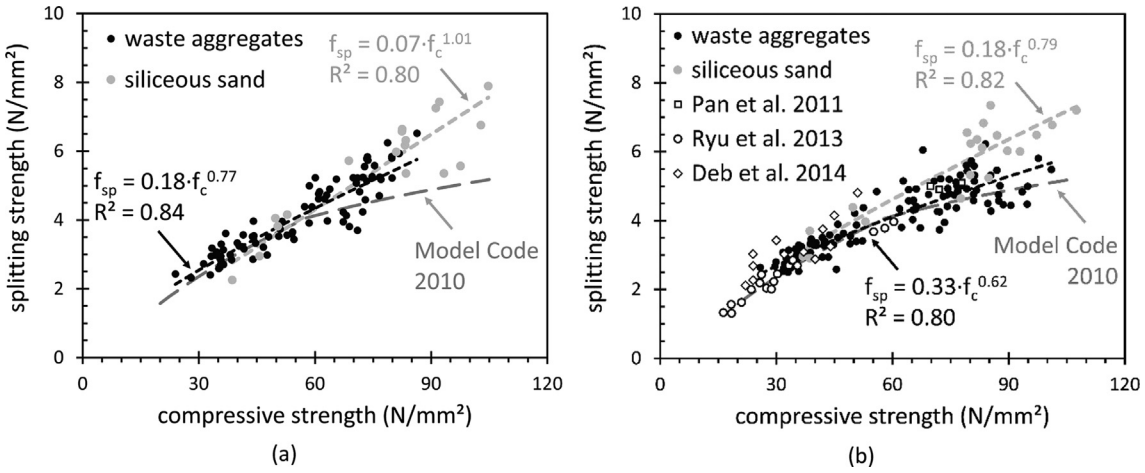

Fig. 13. Splitting versus compressive strength at 7 days (a) and 28 days (b), with superimposed data on geopolymer concrete from literature. Error bars are not reported for the sake of readability.

Table 10
Results of the least squares fitting compared to Model Code provisions, with coefficient of determination (R^2) and Root Mean Square Error (RMSE).

Aggregate type	7-day power law				7-day MC2010		28-day power law				28-day MC2010	
	C_1	C_2	R^2	RMSE	R^2	RMSE	C_1	C_2	R^2	RMSE	R^2	RMSE
Concrete waste	0.111	0.895	0.720	0.487	0.065	0.891	0.245	0.688	0.534	0.534	0.395	0.609
Fired clay waste	0.418	0.572	0.408	0.507	0.208	0.586	0.768	0.413	0.349	0.443	0.311	0.456
Mixed waste	0.197	0.756	0.870	0.302	0.717	0.446	0.303	0.640	0.830	0.350	0.765	0.412
All waste	0.183	0.774	0.835	0.437	0.660	0.627	0.328	0.617	0.799	0.439	0.762	0.478
Siliceous sand	0.069	1.011	0.795	0.689	0.071	1.466	0.183	0.789	0.821	0.565	<0	1.368

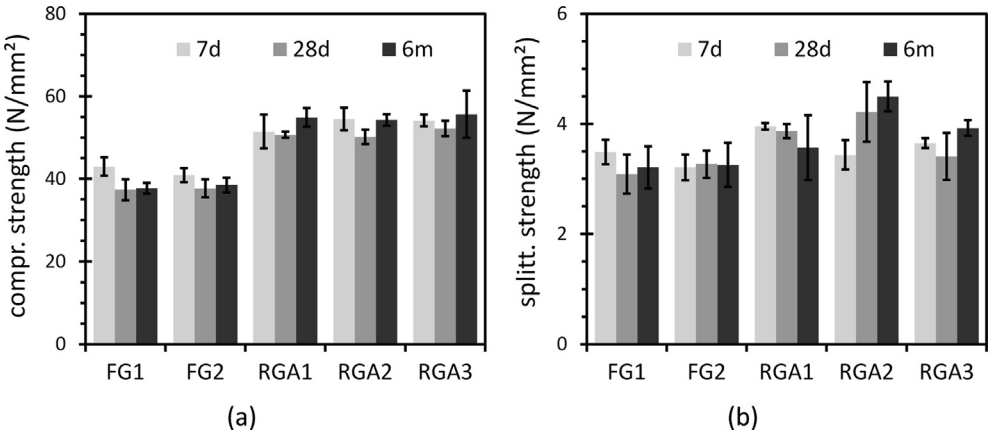

Fig. 14. Compressive (a) and splitting (b) strength measured for mixtures with waste geopolymer aggregates, compared to FG1 and FG2. Error bars represent ± 1 standard deviation.

7. Recyclability of geopolymers as waste aggregates

With the aim of exploring a possible end-of-life pathway, the reuse of tested materials as waste aggregates for new geopolymers was preliminarily assessed from a mechanical standpoint. Previous experiences indicated that the bond between fresh and untreated hardened geopolymer is generally poor or even null, being this a potential hindrance for this type of application.

As anticipated in section 2.1.2, three batches of waste geopolymer aggregates (RG1, RG2 and RG3) were obtained from residual specimens tested in previous and ongoing researches, mostly coming from mixtures with 50% of waste or siliceous sand aggregates. RG3 derived from mixtures REF_wCR2/3 and FG2_CR2/3 made with ordinary Portland cement concrete waste CR2 and CR3, while it was not possible to distinguish the nature of binder and aggregates milled for RG1 and RG2, which however included mostly geopolymers with 50%dw of either waste or siliceous sand aggregates. Three mixtures, one for each waste, were prepared according to the final recipe FG, with the only difference that aggregates were included with the PSD resulting from milling (Fig. 1), with no modifications.

Results (Fig. 14) were better than expected. The performance (between 50–52 N/mm^2 at 28 days and 54–56 N/mm^2 at 6 months in compression; between 3.4–4.2 N/mm^2 at 28 days and 3.6–4.5 N/mm^2 at 6 months in indirect tension) was comparable to the reference materials in terms of strength, and was not remarkably sensitive to the input geopolymer waste. Outcomes suggested that the mechanical action of crushing and milling might be enough to

allow geopolymers exploiting their potential as recycled aggregates. The observed improvement (about 40% in compression and 20% in indirect tension at 6 months, in average) might be partly attributed to a more balanced PSD of geopolymer waste aggregates compared to that of FG mixtures (Fig. 1), despite a slightly lower apparent density (approximately −3%), while porosity was either similar or slightly greater (2–10%). The encouraging results fostered an ongoing dedicated investigation, which will involve a characterization of the aggregate-binder interface, leaching aspects and Life Cycle Assessment analyses in the light of a cradle-to-cradle scenario.

8. Conclusions

A metakaolin-slag-fly ash-potassium silicate geopolymer mortar, embedding about 50% of dry weight of CDW aggregates, was developed within the Horizon 2020 InnoWEE project. The recipe was optimized through a trial and error approach to deliver acceptable prototype panels and to comply with requirements of the pilot plant.

The fresh paste at 23 °C had a suitable viscosity (120–150 Pa·s), whereas the hardened material delivered a satisfactory strength (about 38 N/mm^2 in compression and 3.2 N/mm^2 in indirect tension after 6 months), achieved with molar ratios Si/Al ≈ 2.3 and K/Al ≈ 0.75, water content ≈ 19.6%, and combining a fine recycled aggregate sand (0–1 mm) with a coarser one (1–2 mm) in 1:2 proportion. The use of a relatively small amount (5.9% of dry weight) of class F fly ash was proven effective in ensuring an open time greater than 1 h in reasonable operative conditions (70 min at 23 °C), without hindering the possibility of hardening at ambient temperature (about 20 °C), likely fostered by the presence of Ca oxides in the furnace slag, and with no detriment to the mechanical performance.

The presence of fired clay waste aggregates, at least with reference to mortar-like materials, was proven beneficial from a strength point of view, compared to the exclusive use of waste concrete.

Effects of drying shrinkage were effectively counteracted by setting a 12 h curing temperature of 50 °C followed, after demoulding, by a 6 day curing at ambient temperature in a moist environment (preferably in a sealed envelope), and by adding 1.5‰ of dry weight of polypropylene fibres 6 mm long.

The long-term behaviour, up to 6–12 months, showed a substantial stability of tested materials, suggesting the suitability of 28 days as a possible reference age for mechanical testing. A distinctive behaviour of geopolymer mortars during the drying shrinkage was highlighted in comparison to lime and cement-based products, pointing out also the occurrence of daily fluctuations of shrinkage and swelling, due to variations of air humidity, which can be caught only by frequent measures (at least 4–6 every 24 h).

The effect of specimen diameter (22 or 35 mm) and aspect ratio (0.25–3) on compressive strength was explored for the final mixtures, providing empirical indications on the average strength of larger specimens (e.g. 40–50 mm) to be expected based on 22 mm results. The relation between splitting and compressive strength was investigated through results of about 130 mixtures tested so far in past and ongoing researches. Outcomes suggest the consistency of tested geopolymers with the current knowledge about brittle and quasi-brittle materials like mortar, concrete and rocks.

Lastly, a preliminary evaluation of the recyclability of geopolymers as aggregates in a new geopolymer production was carried out from a mechanical standpoint, assessing their potential reuse in a closed loop process.

CRediT authorship contribution statement

Matteo Panizza: Methodology, Investigation, Formal analysis, Visualization, Writing - original draft. **Marco Natali:** Conceptualization, Investigation, Supervision, Writing - review & editing. **Enrico Garbin:** Methodology, Validation, Writing - review & editing. **Vilma Ducman:** Methodology, Writing - review & editing. **Sergio Tamburini:** Conceptualization, Investigation, Supervision, Writing - review & editing.

Declaration of Competing Interest

The authors declare that they have no known competing financial interests or personal relationships that could have appeared to influence the work reported in this paper.

Acknowledgements

This research has received funding from the European Union's Horizon 2020 research and innovation programme under grant agreement No. 723916 (Project H2020-EEB-2016 InnoWEE, G.A. 723916). Inorganic waste aggregates were processed and supplied by Guidolin Giuseppe – ECO G. (Castelfranco Veneto – TV, Italy). Advanced Management Solutions – AMS (Athens, Greece) designed the pilot plant, scaled up the production process, and manufactured the panels for quality testing and for installation in demo sites (the one located in Padova is shown in the graphical abstract). Minerali Industriali (Novara, Italy) is acknowledged for having supplied metakaolin (in agreement with Imerys S.A., Paris, France) and furnace slag. Crosfield Italia (Verona, Italy) provided potassium silicate solutions.

References

[1] Eurostat Yearbook: The Statistical Guide to Europe. Office for the Official Publications of the European Communities, Luxembourg, 2019. Online publication, data retrieved on 20 June 2019.
[2] JRC Report EUR 24918 EN 2011. Supporting Environmentally Sound Decisions for Construction and Demolition (C&D) Waste Management – A practical guide to Life Cycle Thinking (LCT) and Life Cycle Assessment (LCA). European Commission Joint Research Centre (2011). doi:10.2788/54618.
[3] F. Pacheco-Torgal, V. Tam, J. Labrincha, Y. Ding, J. de Brito (Eds.), Handbook of Recycled Concrete and Demolition Waste, Woodhead Publishing, Cambridge, UK, 2013.
[4] Directive 2008/98/EC of the European Parliament and of the Council of 19 November 2008 on waste and repealing certain Directives. Official Journal of the European Union no. L 312, 3-30.
[5] C.-L. Peng, D.E. Scorpio, C.J. Kibert, Strategies for successful construction and demolition waste recycling operations, Constr. Manage. Econ. 15 (1997) 49–58, https://doi.org/10.1080/014461997373105.
[6] R.H. Paul, R. Warwik, Use of recycled crushed concrete for road pavement subbase, in: Roads '96 Conference Proceedings. Christchurch, New Zealand, 1996, pp. 93–106.
[7] P.J. Nixon, Recycled concrete as an aggregate for concrete—a review, Mater. Struct. 11 (5) (1978) 371–378, https://doi.org/10.1007/BF02473878.
[8] T.C. Hansen, Recycled aggregates and recycled aggregate concrete second state-of-the-art report developments 1945–1985, Mater. Struct. 19 (1986) 201–246, https://doi.org/10.1007/BF02472036.
[9] M. Behera, S.K. Bhattacharyya, A.K. Minocha, R. Deoliya, S. Maiti, Recycled aggregate from C&D waste & its use in concrete – A breakthrough towards sustainability in construction sector: A review, Constr. Build. Mater. 68 (2014) 501–516, https://doi.org/10.1016/j.conbuildmat.2014.07.003.
[10] N. Otsuki, S. Miyazato, W. Yodsudjai, Influence of recycled aggregate on interfacial transition zone, strength, chloride penetration and carbonation of concrete, J. Mater. Civil Eng. 15 (2003) 443–451, https://doi.org/10.1061/(ASCE)0899-1561(2003)15:5(443).
[11] C.S. Poon, Z.H. Shui, L. Lam, Effect of microstructure of ITZ on compressive strength of concrete prepared with recycled aggregates, Constr. Build. Mater. 18 (2004) 461–468, https://doi.org/10.1016/j.conbuildmat.2004.03.005.
[12] S. Manzi, C. Mazzotti, M.C. Bignozzi, Short and long-term behavior of structural concrete with recycled concrete aggregate, Cem. Concr. Compos. 37 (2013) 312–318, https://doi.org/10.1016/j.cemconcomp.2013.01.003.
[13] W. Li, J. Xiao, Z. Sun, S. Kawashima, S.P. Shah, Interfacial transition zones in recycled aggregate concrete with different mixing approaches, Constr. Build.

Mater. 35 (2012) 1045–1055, https://doi.org/10.1016/j.conbuildmat.2012.06.022.
[14] J. Xiao, W. Li, Z. Sun, D.A. Lange, S.P. Shah, Properties of interfacial transition zones in recycled aggregate concrete tested by nanoindentation, Cem. Concr. Compos. 37 (2013) 276–292, https://doi.org/10.1016/j.cemconcomp.2013.01.006.
[15] J. Xiao, W. Li, D.J. Corr, S.P. Shah, Effects of interfacial transition zones on the stress–strain behavior of modeled recycled aggregate concrete, Cem. Concr. Res. 52 (2013) 82–99, https://doi.org/10.1016/j.cemconres.2013.05.004.
[16] T. Hansen (Ed.), Recycling of Demolished Concrete and Masonry, CRC Press, London, 1992. doi:10.1201/9781482267075.
[17] F.M. Khalaf, A.S. DeVenny, Properties of new and recycled clay brick aggregates for use in concrete, J MATER CIVIL ENG 17 (4) (2005) 456–464, https://doi.org/10.1061/(ASCE)0899-1561(2005)17:4(456).
[18] I. Kesegić, I. Netinger, D. Bjegović, Recycled clay brick as an aggregate for concrete: overview, TEH VJESN 15 (3) (2008) 35–40.
[19] Y. Wu, B. Lu, T. Bai, H. Wang, F. Du, Y. Zhang, L. Cai, C. Jiang, W. Wang, Geopolymer, green alkali activated cementitious material: Synthesis, applications and challenges, Constr. Build. Mater. 224 (2019) 930–949, https://doi.org/10.1016/j.conbuildmat.2019.07.112.
[20] N.R. Rakhimova, R.Z. Rakhimov, Literature review of advances in materials used in development of alkali-activated mortars, concretes, and composites, J. Mater. Civil Eng. 31 (11) (2019) 03119002, https://doi.org/10.1061/(ASCE)MT.1943-5533.0002899.
[21] J.S.J. van Deventer, J.L. Provis, P. Duxson, G.C. Lukey, Reaction mechanisms in the geopolymeric conversion of inorganic waste to useful products, J. Hazard. Mater. 139 (2007) 506–513, https://doi.org/10.1016/j.jhazmat.2006.02.044.
[22] F. Pacheco-Torgal, J. Labrincha, C. Leonelli, A. Palomo, P. Chindaprasit (Eds.), Handbook of Alkali-Activated Cements, Mortars and Concretes, Elsevier, 2014. ISBN: 9781782422761.
[23] A. Vásquez, V. Cárdenas, R.A. Robayo, R.M. de Gutiérrez, Geopolymer based on concrete demolition waste, Adv. Powder Technol. 27 (4) (2016) 1173–1179, https://doi.org/10.1016/j.apt.2016.03.029.
[24] S. Ahmari, X. Ren, V. Toufigh, L. Zhang, Production of geopolymeric binder from blended waste concrete powder and fly ash, Constr. Build. Mater. 35 (2012) 718–729, https://doi.org/10.1016/j.conbuildmat.2012.04.044.
[25] M.F. Zawrah, R.A. Gado, N. Feltin, S. Ducourtieux, L. Devoille, Recycling and utilization assessment of waste fired clay bricks (Grog) with granulated blast-furnace slag for geopolymer production, Process Saf. Environ. 103 (2016) 237–251, https://doi.org/10.1016/j.psep.2016.08.001.
[26] A. Allahverdi, E.N. Kani, Use of construction and demolition waste (CDW) for alkali-activated or geopolymer cements, in: Handbook of recycled concrete and demolition waste, Woodhead Publishing Limited, 2013, pp. 439–475. ISBN 978-0-85709-682-1.
[27] A. Allahverdi, E. Najafi Kani, Construction wastes as raw materials for geopolymer binders, Int. J. Civil Eng. 7 (3) (2009) 154–160.
[28] R.A. Robayo-Salazar, J.F. Rivera, R.M. de Gutiérrez, Alkali-activated building materials made with recycled construction and demolition wastes, Constr. Build. Mater. 149 (2017) 130–138, https://doi.org/10.1016/j.conbuildmat.2017.05.122.
[29] D. Zaharaki, M. Galetakis, K. Komnitsas, Valorization of construction and demolition (C&D) and industrial wastes through alkali activation, Constr. Build. Mater. 121 (2016) 686–693, https://doi.org/10.1016/j.conbuildmat.2016.06.051.
[30] K. Komnitsas, D. Zaharaki, A. Vlachou, G. Bartzas, M. Galetakis, Effect of synthesis parameters on the quality of construction and demolition wastes (CDW) geopolymers, Adv. Powder Technol. 26 (2) (2015) 368–376, https://doi.org/10.1016/j.apt.2014.11.012.
[31] R.A. Robayo-Salazar, J.M. Mejía-Arcila, R.M. de Gutiérrez, Eco-efficient alkali-activated cement based on red clay brick wastes suitable for the manufacturing of building materials, J. Clean. Prod. 166 (2017) 242–252, https://doi.org/10.1016/j.jclepro.2017.07.243.
[32] L. Reig, M.M. Tashima, M.V. Borrachero, J. Monzó, C.R. Cheeseman, J. Payá, Properties and microstructure of alkali-activated red clay brick waste, Constr. Build. Mater. 43 (2013) 98–106, https://doi.org/10.1016/j.conbuildmat.2013.01.031.
[33] F. Puertas, A. Barba, M.F. Gazulla, M.P. Gómez, M. Palacios, S. Martínez-Ramírez, Ceramic wastes as raw materials in Portland cement clinker fabrication: characterization and alkaline activation, Materiales de Construcción 56 (281) (2006) 73–84, https://doi.org/10.3989/mc.2006.v56.i281.94.
[34] Z. Sun, H. Cui, H. An, D. Tao, Y. Xu, J. Zhai, Q. Li, Synthesis and thermal behavior of geopolymer-type material from waste ceramic, Constr. Build. Mater. 49 (2013) 281–287, https://doi.org/10.1016/j.conbuildmat.2013.08.063.
[35] Directive 2010/31/EU of the European Parliament and of the Council of 19 May 2010 on the energy performance of buildings. Official Journal of the European Union no. L 153, 13–35.
[36] M. Panizza, M. Natali, E. Garbin, S. Tamburini, M. Secco, Assessment of geopolymers with Construction and Demolition Waste (CDW) aggregates as a building material, Constr. Build. Mater. 181 (2018) 119–133, https://doi.org/10.1016/j.conbuildmat.2018.06.018.
[37] Frankovič A., Ducman V., Dolenec S., Panizza M., Tamburini S., Natali M., Pappa M., Tsoutis C., Bernardi A., Up-scaling and performance assessment of façade panels produced from construction and demolition waste using alkali activation technology, Constr. Build. Mater., Submitted for publication.
[38] J.L. Provis, J.S.J. van Deventer (Eds.), Alkali Activated Materials. State-of-the-Art Report, RILEM TC 224-AAM, Springer, 2014. ISBN 978-94-007-7671-5. doi:10.1007/978-94-007-7672-2.
[39] EU Commission Decision of 18 December 2014 n. 2014/955/EU. Official Journal of the European Union n. L 370/44 of 30.12.2014.
[40] EN 933-2. Tests for geometrical properties of aggregates. Determination of particle size distribution. Test sieves, nominal size of apertures. European Committee for Standardization (1996).
[41] EN 12390-3. Testing Hardened Concrete-Part 3: Compressive strength of test specimens. European Committee for Standardization (2011).
[42] EN 12390-6. Testing Hardened Concrete-Part 6: Tensile splitting strength of test specimens. European Committee for Standardization (2000).
[43] EN 12390-5. Testing hardened concrete-Part 5: Flexural strength of test specimens. European Committee for Standardization (2009).
[44] ASTM C20-00. Standard Test Methods for Apparent Porosity, Water Absorption, Apparent Specific Gravity, and Bulk Density of Burned Refractory Brick and Shapes by Boiling Water. ASTM International, formerly American Society for Testing and Materials (2010).
[45] C. Kuenzel, L.J. Vandeperre, S. Donatello, A.R. Boccaccini, C. Cheeseman, Ambient temperature drying shrinkage and cracking in metakaolin-based geopolymers, Am. Ceram. Soc. Bull. 95 (10) (2012) 3270–3277, https://doi.org/10.1111/j.1551-2916.2012.05380.x.
[46] J. Davidovits, Geopolymer Chemistry and Applications, 3rd ed., Geopolymer Institute, Saint-Quentin (France), 2011.
[47] EN 1990 Eurocode – Basis of structural design. European Committee for Standardization (2005).
[48] J.G.M. van Mier, S.P. Shah, M. Arnaud, J.P. Balayssac, A. Bascoul, et al., Strain-softening of concrete in uniaxial compression, Mater. Struct. 30 (4) (1997) 195–209, https://doi.org/10.1007/BF02486177.
[49] EN 1996-1-1 Eurocode 6 – Design of masonry structures. General rules for reinforced and unreinforced masonry structures. European Committee for Standardization (2005).
[50] EN 1015-11. Methods of test for mortar for masonry-Part 11: Determination of flexural and compressive strength of hardened mortar. European Committee for Standardization (1999).
[51] R.C. Meininger, F.T. Wagner, K.W. Hall, Concrete core strength–The effect of length to diameter ratio, J. Test. Eval. 5 (3) (1977) 147–153, https://doi.org/10.1520/JTE11631J.
[52] J.H. Bungey, Determining concrete strength by using small-diameter cores, Mag. Concr. Res. 31 (107) (1979) 91–98, https://doi.org/10.1680/macr.1979.31.107.91.
[53] W.K. Yip, C.T. Tam, Concrete strength evaluation through the use of small diameter cores, Mag. Concr. Res. 40 (143) (1988) 99–105, https://doi.org/10.1680/macr.1988.40.143.99.
[54] F. Indelicato, A proposal for the prediction of the characteristic cube strength of concrete from tests on small cores of various diameters, Mater. Struct. 31 (4) (1998) 242–246, https://doi.org/10.1007/BF02480422.
[55] A.O. Celik, K. Kilinc, M. Tuncan, A. Tuncan, Distributions of compressive strength obtained from various diameter cores, ACI Mater. J. 109 (6) (2012) 597–606, https://doi.org/10.14359/51684157.
[56] N. Turk, W.R. Dearman, A correction equation on the influence of length-to diameter ratio on the uniaxial compressive strength of rocks, Eng. Geol. 22 (3) (1986) 293–300, https://doi.org/10.1016/0013-7952(86)90030-X.
[57] A.B. Hawkins, Aspects of rock strength, Bull. Eng. Geol. Environ. 57 (1) (1998) 17–30, https://doi.org/10.1007/s100640050017.
[58] E. Tuncay, N. Hasancebi, The effect of length to diameter ratio of test specimens on the uniaxial compressive strength of rock, Bull. Eng. Geol. Environ. 68 (4) (2009) 491–497, https://doi.org/10.1007/s10064-009-0227-9.
[59] W.J. Darlington, P.G. Ranjith, S.K. Choi, The effect of specimen size on strength and other properties in laboratory testing of rock and rock-like cementitious brittle materials, Rock Mech. Rock Eng. 44 (5) (2011) 513–529, https://doi.org/10.1007/s00603-011-0161-6.
[60] Bureau of Reclamation Concrete Manual Part 2 (9th ed.), U.S. Government Printing Office, Washington, DC (1992).
[61] A.M. Neville, J.J. Brooks, Concrete Technology, 2nd ed., Prentice Hall, UK, 1987. ISBN 9780273732198.
[62] S. Wolinski, D.A. Hordijk, H.W. Reinhardt, H.A. Cornelissen, Influence of aggregate size on fracture mechanics parameters of concrete, Int. J. Cem. Compos. Lightweight Concr. 9 (2) (1987) 95–103, https://doi.org/10.1016/0262-5075(87)90025-X.
[63] S. Enterprises, Scilab: Free and Open Source software for numerical computation (OS Windows© Version 6.0.1) [Software], http://www.scilab.org, last accessed 2019/07/31.
[64] T. Kvalseth, Cautionary Note about R^2, Am. Stat. 39 (4) (1985) 279–285, https://doi.org/10.2307/2683704.
[65] Z.P. Bažant, Design of quasibrittle materials and structures to optimize strength and scaling at probability tail: an apercu, Proc. R. Soc. A 475 (2019) 20180617, https://doi.org/10.1098/rspa.2018.0617.
[66] Z.P. Bažant, Y. Xiang, Size effect in compression fracture: splitting crack band propagation, J. Eng. Mech. 123 (2) (1997) 162–172, https://doi.org/10.1061/(ASCE)0733-9399(1997)123:2(162).
[67] Z.P. Bazant, D. Novák, (2001). Nonlocal Weibull theory and size effect in failures at fracture initiation, in: Proc. of Fracture Mechanics of Concrete Structures–FraMCoS-4, Chachan-Paris (France), 659–664.

[68] R. Jasiński, Ł. Drobiec, W. Mazur, Validation of selected non-destructive methods for determining the compressive strength of masonry units made of autoclaved aerated concrete, Materials 12 (3) (2019) 389, https://doi.org/10.3390/ma12030389.
[69] M.A. van Vliet, J.M. van Mier, Experimental investigation of concrete fracture under uniaxial compression, Mech. Cohes-Frict. Mater. 1 (1) (1996) 115–127, https://doi.org/10.1002/(SICI)1099-1484(199601)1:1%3C115::AID-CFM6%3E3.0.CO;2-U.
[70] fib Bulletin No. 65 (2012). Model Code 2010 - Final draft, Vol. 1. Int. Federation for Structural Concrete (fib). Lausanne, Switzerland. ISBN 978-2-88394-105-2.
[71] G.A. Parsekian, F.S. Fonseca, G.L. Pinheiro, J.S. Camacho, Properties of mortar using cubes, prism halves, and cylinder specimens, ACI Mater. J. 111 (4) (2014) 443–454, https://doi.org/10.14359/51686726.
[72] C. Rocco, G.V. Guinea, J. Planas, M. Elices, Review of the splitting-test standards from a fracture mechanics point of view, Cem. Concr. Res. 31 (2001) 73–82, https://doi.org/10.1016/S0008-8846(00)00425-7.
[73] Z. Pan, J.G. Sanjayan, B.V. Rangan, Fracture properties of geopolymer paste and concrete, Mag. Concr. Res. 63 (10) (2011) 763–771, https://doi.org/10.1680/macr.2011.63.10.763.
[74] G.S. Ryu, Y.B. Lee, K.T. Koh, Y.S. Chung, The mechanical properties of fly ash-based geopolymer concrete with alkaline activators, Constr. Build. Mater. 47 (2013) 409–418, https://doi.org/10.1016/j.conbuildmat.2013.05.069.
[75] P.S. Deb, P. Nath, P.K. Sarker, The effects of ground granulated blast-furnace slag blending with fly ash and activator content on the workability and strength properties of geopolymer concrete cured at ambient temperature, Mater. Des. 62 (2014) 32–39, https://doi.org/10.1016/j.matdes.2014.05.001.